Published in final edited form as:
Ann N Y Acad Sci. 2008 ; 1131: 13–36. doi:10.1196/annals.1413.002.

New Horizons for Imaging Lymphatic Function

Ruchi Sharma[a,b], **Juliet A. Wendt**[a,b], **John C. Rasmussen**[b], **Kristen E. Adams**[b], **Milton V. Marshall**[b], and **Eva M. Sevick-Muraca**[a,b]

[a] Translational Biology and Molecular Medicine, Baylor College of Medicine, Houston, Texas, USA

[b] Division of Molecular Imaging, Department of Radiology, Baylor College of Medicine, Houston, Texas, USA

Abstract

In this review, we provide a comprehensive summary of noninvasive imaging modalities used clinically for the diagnosis of lymphatic diseases, new imaging agents for assessing lymphatic architecture and cancer status of lymph nodes, and emerging near-infrared (NIR) fluorescent optical imaging technologies and agents for functional lymphatic imaging. Given the promise of NIR optical imaging, we provide example results of functional lymphatic imaging in mice, swine, and humans, showing the ability of this technology to quantify lymph velocity and frequencies of propulsion resulting from the contractility of lymphatic structures.

Keywords

lymph flow; NIR optical imaging; fluorescence; indocyanine green

Introduction

Many of the recent advances in the field of lymphovascular research can be ascribed to the discovery of lymphatic endothelium–specific biomarkers that enable identification of lymphatics. Yet there are few noninvasive, *in vivo* imaging modalities to visualize and quantitatively assess functional lymphatic vasculature within subjects, whether animal or human. The ability to noninvasively image functional lymphatics and markers of lymphangiogenesis could have an impact on our understanding of a number of diseases in which the lymphatic system is implicated, such as cancer metastases,[1] asthma,[2] diabetes,[3] and obesity.[4] Imaging could further play an important role in elucidating the role of lymphatics, not only in disease, but in health as well. In comparison to the hemovascular system, comparatively little is known about the lymphatic system, probably because of the inability to readily image the lymphatics. For example, while arteriovenous malformations (AVMs) are readily assessed with angiographic techniques, there are few available imaging techniques to assess lymphovascular malformations or even to discern whether lymphovascular malformations present with AVMs. In short, there is a paucity of imaging techniques to assess lymphatic function *in vivo*.

Address for correspondence: Eva M. Sevick-Muraca, Division of Molecular Imaging, Baylor College of Medicine, One Baylor Plaza, BCM 360, Houston, TX 77030. Voice: +1-713-798-3684; fax: +1-713-798-2749. evas@bcm.edu.

Conflicts of Interest
The authors declare no conflicts of interest.

Here we review the imaging modalities used clinically and in animal studies as well as those under development in order to provide a "state of the art" review of new horizons in noninvasive, lymphatic imaging. In the first section, we begin with conventional imaging modalities of X-ray, nuclear, magnetic resonance imaging (MRI), and ultrasound (US) and focus upon their clinical use as well as their associated new experimental imaging agents currently under development. Next, the emerging developments in optical imaging modality are summarized and the enhanced sensitivity of near-infrared (NIR) optical imaging for imaging lymphatic function, lymph flow, and propulsion from contractile lymphangions is described. Examples of NIR fluorescence optical imaging within mice, swine, and humans are provided, demonstrating its unique ability to show lymphatic function. Finally, we describe work using labeled hyaluronan as a molecular "stain" that targets the LYVE-1 receptor and that may provide useful images of lymphatic architecture for therapy, surgical planning, and use in an intraoperative setting.

It is hoped that with an emerging armamentarium that allows the noninvasive imaging of lymphatic function and architecture, a new understanding will be gained of lymphatic biology, new means of therapeutic modulation of lymphatic function will be developed, and more effective diagnoses of lymphatic diseases will be enabled.

Modalities for Lymph Imaging

Imaging of the hemovascular system typically requires the administration of milliliters of contrast agents that are injected intravenously for direct imaging of the arteriovenous systems. However, there is no simple route for administration of milliliter volumes of contrast agents into the lymphatic system. The dermis of the skin is made up of blind-ended initial lymphatics that serve as an entry portal for particles, cells, and interstitial fluid. Under a positive pressure gradient, these initial lymphatics distend, creating openings between loosely anchored endothelial cells that further allow in-flux of fluid and particulate matter from extracellular space.[5] Lymph drainage from these initial lymphatics is received by deeper collecting vessels that contain valves to maintain unidirectional flow of lymph. These collecting vessels are surrounded by smooth muscle cells that rhythmically contract to propel lymph to lymph nodes. As described below and in Figure 1, there are four distinct routes to introduce imaging agents into the lymphatic space: (i) intradermally for delivery into the lymphatic vessels via the lymph plexus in the dermis; (ii) subcutaneously into the interstitium for permeation into the lymphatic capillaries and vessels; (iii) directly introducing agents into the lymphatic space through lymphatic vessel cannulation; and (iv) intravenously for transit from the vascular space to the interstitium for permeation into the lymphatics or for direct deposition via the microcirculation found within the lymph nodes. Particles less than a few nanometers (~11 nm) in size can pool into the lymph nodes via blood circulation, but can also diffuse into lymphatic vessels via the gap junctions between the endothelial cells under a hydrostatic pressure gradient.[6] Particles as large as 100 nm in diameter extravasate into the interstitial space, where they are phagocytosed by macrophages and are then transported to lymph nodes. Particles larger than 100 nm typically remain trapped in the interstitium.[7]

The following sections in this chapter are limited to lymphatic imaging modalities employed for whole-animal or patient imaging that employs contrast agents. While microscopy studies of lymphatic function in animal preparations has enabled significant understanding of the lymphovascular system, their translation to clinical use may be doubtful because of the restricted depth of tissue studied. In the following, we focus upon X-ray, nuclear, MRI, US, and NIR optical imaging modalities.

X-Ray-Based Techniques

X-ray imaging provides the most common form of hemovascular imaging. High-energy X-rays, which span the electromagnetic spectrum from 0.001 to 10 nm,[8] have a low soft-tissue attenuation coefficient. By introducing a contrast agent into the vasculature which absorbs X-rays, two-dimensional projections containing transmission shadows of vascular architecture are acquired. A series of projection images can then be tomographically rendered, using computed tomography (CT) to produce a three-dimensional image of the vasculature. Vascular imaging of blood vessels, or angiography, is established in the clinic, while lymphangiography is more complex.

Lymphangiography involves the direct administration of an iodinated contrast agent into a cannulated lymph vessel for radiography or CT of lymphatic architecture. Hultén *et al.*[9] and Kinmonth[10,11] first reported the use of blue dye administered interdigitally in hands or in feet to find, dissect, and cannulate lymphatic vessels for subsequent infusion of a contrast agent to detect lymphatic vasculature by serial radiography. Hultén *et al.*[9] also utilized subcutaneous injection of a blue dye to identify and cannulate lymphatic vessels in the arms of patients with breast carcinoma. The cannulated lymphatic vessels were then infused with 4–7 mL of Lipiodol (Guerbet, Aulnay-Sous-Bois, France), an oily contrast agent used to detect lymph nodes. Recently, lymphangiography was employed to detect postoperative lymphatic leakage in patients with known or suspected lymphocele, chylothorax, or lymphatic fistulas.[12] Figure 2 shows an X-ray scan taken after injection of up to 14 mL of Lipidiol. The pedal lymphangiography depicts a lymphatic fistula (arrows) in a patient who underwent resection of melanoma in the right thigh and inguinal lymphadenectomy.[12] Although lymphangiography enables imaging of lymph vessels and lymph nodes,[13,14] it has been largely abandoned because of such complications as infection, lung embolization, pulmonary edema, respiratory distress, and damage to the lymphatics, as well as the technical skill required to cannulate lymph vessels.[15–17]

As an alternative to direct injection into the lymphatic space, water-soluble iodinated contrast agents can be delivered intradermally for subsequent lymphatic uptake in an indirect lymphangiography technique. Partsch and co-workers[18,19] administered up to 20 mL of Iotasul (Schering AG, Berlin, Germany), a nonionic water-soluble contrast agent, into the interdigital or intradermal space of patients with lymphedema in order to visualize the dermal lymphatics that were too small to be cannulated. The technique avoids the complexity and invasiveness of direct injection into the lymphatic space,[20] but is restricted by the small volume (~0.2 mL) of fluid that can occupy the dermal tissues at each injection site.

Iopamidol, another water-soluble nonionic contrast agent, has also been employed to visualize breast and esophagogastric tract lymph drainage pathways. CT lymphangiography using subcutaneous injections of up to 1 mL of undiluted iopamidol in 10 female dogs enabled visualization of breast lymph pathways, 20 sentinel lymph nodes, and 110 distant nodes.[21] In addition, CT lymphangiography following endoscope-guided administration of 2 mL of Iopamidol (Nihon Schering, Osaka, Japan) into the esophageal or gastric submucosal space of nine dogs enabled visualization of lymphatic channels draining into regional lymph nodes (possibly sentinel lymph nodes), hence demonstrating the technique's potential to aid surgeons in the surgical planning of the extent of lymph node dissection. This imaging agent has also been demonstrated for esophageal cancer staging by Suga and coworkers,[22] as depicted in Figure 3, which illustrates transverse and sagittal CT lymphangiograms of a patient with middle-thoracic esophageal cancer. An endoscope was used to administer 2 mL of iopamidol in the peritumoral submucosal space. The CT lymphangiogram identified a short lymphatic vessel (unlabeled arrow in Fig. 3B) at a paraesophageal region draining into a middle-thoracic paraesophageal lymph node. The patient underwent esophagectomy and

regional lymphadenectomy, including the unenhanced lymph nodes, which were later found to be positive for micrometastases. These images demonstrate the ability of CT lymphangiography to detect sentinel lymph nodes from the lymphatic drainage routes around the tumor. The potential of CT lymphangiography to possibly detect malignant lymph nodes was demonstrated by Wisner *et al.*,[23] who administered 2 mL per subcutaneous injection (6–12 mL total) of a 15% wt/vol of an iodinated suspension in swine with melanoma. Reviews of CT scans revealed differences in iodine concentration and lymph node morphology in diseased as compared to the normal lymph nodes, suggesting that the use of the iodinated contrast enhanced CT to identify malignant lymph nodes. However, once within the lymphatic compartment, the iodinated contrast agents approved for human use drain rapidly to the blood vascular compartment and clear from the body, limiting the time for imaging and their clinical usefulness. In addition, the millimolar tissue agent concentrations needed to produce X-ray image contrast make their use difficult when administered in limited volumes within the dermal space.

A number of experimental CT agents are currently under development as a result of these limitations. Novel bismuth sulfide nanoparticles with a longer hemovascular circulation half-life may address the clearance issues of current iodinated CT contrast agents In an experimental study by Rabin *et al.*,[24] 50 μL of polymer-coated bismuth sulfide nanoparticles with a hydrodynamic diameter of 30 ± 10 nm and corresponding to 11.4 μmol Bi^{3+} were subcutaneously injected and imaged for up to 140 h in mice. The images depicted contrast-enhanced lymph nodes. Although CT imaging of long-circulating bismuth sulfide nanoparticles can be achieved at low volumes and with efficacies comparable to that of iodinated agents, concerns regarding fate and long-term toxicity may hinder future clinical translation.

Because of the difficulties of delivering sufficient amounts of agents necessary to produce X-ray contrast, lymphangiography is not routinely used for diagnosis of lymphatic disorders and does not have the clinical diagnostic impact of hemovascular angiography.

Nuclear Imaging

Nuclear imaging techniques employ radionuclides as contrast agents which, upon decay, generate either gamma photons of ~0.0001-nm wavelength[8] or positrons that annihilate to produce two 511-kEV photons at 22-nm wavelength. Gamma photons and annihilation photons can propagate efficiently and have low attenuation in tissues. Gamma scintigraphy is the most common nuclear imaging in which gamma photons are detected for the generation of a two-dimensional planar image detailing the position of the radionuclide. While scintigraphy provides two-dimensional images, single-photon emission computed tomography (SPECT) reconstructs three-dimensional positions of radionuclide sources within the body from a series of images acquired by a gamma camera that is rotated around the subject. However, since the technique requires pinhole rejection of scattered gamma photons, a large number of photons remain undetected in SPECT, and scanning times can be long. Conversely, positron emission tomography (PET) depends upon coincident detection of the annihilation photons for three-dimensional reconstruction of the position of positron annihilation. Unlike X-ray-based contrast agents, nuclear techniques, such as gamma scintigraphy, SPECT, and PET, are associated with exquisite sensitivity because of the ability to image tissues with pico- to femtomolar tissue concentrations of radionuclides. The enhanced sensitivity enables intradermal administration of small volumes and concentrations of radiopharmaceuticals for lymphatic delivery.

Lymphoscintigraphy—The most common nuclear method of imaging the lymphatics is lymphoscintigraphy. In the United States, lymphoscintigraphy is performed with filtered

99m-technetium (Tc-99m) sulfur colloid (40–100 nm in diameter), whereas in Europe it is performed with Tc-99m albumin nanocolloid (5–80 nm), Tc-99m rhenium colloid (2–15 nm), Tc-99m antimony colloid (3–30 nm), and other soluble noncolloids, such as Tc-99m human serum albumin, 99mTc human immunoglobin, and Tc-99m dextran.[25–27] Typically. intradermal or subcutaneous injections of 11.1–111 MBq (0.3–3 mCi) of filtered Tc-99m sulfur colloid in up to 4 mL of saline solution are administered between 30 min to 2 h prior to imaging; however, administration of radiocolloid can be performed 1 day prior to imaging. The scintigram requires anywhere from 20 min up to 2 h to be acquired. For nodal staging in breast cancer and melanoma, intradermal or subcutaneous injections of radiocolloid are generally done peritumorally or subareolarly (in breast cancer), and gamma scintigraphy is used to identify the draining nodal basins for subsequent resection for pathologic examination for cancer.

Because of the slow depot clearance and incomplete lymph node extraction in sentinel lymph node mapping (SLNM) using Tc-99m-labeled sulfur colloid, several radiopharmaceuticals are under investigation to stage cancer. In Japan, Tc-labeled rhenium colloid (Tc-99m Re, 2–15 nm in diameter) and soluble Tc-99m human serum albumin diethylene-triamine-pentaacetic acid (Tc-99m HSA-D; molecular weight greater than 50,000) have been more widely used than Tc-99m sulfur colloid. Sato and co-workers[28] compared the usefulness of both radiopharmaceuticals for nodal staging. In their study, 65 patients with oral cancer received injections of 0.25 mL of 37 MBq (1 mCi) Tc-99m Re, whereas while 20 received 0.1 mL of 74 MBq (2 mCi) Tc-99m HSA-D for nodal staging. When compared to the soluble Tc-99m HSA-D, Tc-99m Re was found to provide better scintigrams of lymph nodes, presumably because of the preferential uptake of radio-colloids into the lymph nodes while the soluble Tc-99m-HSA-D passed through the lymphatics. However, the radiocolloid required longer times for transit to the lymph nodes than the soluble radiopharmaceutical. Recently, in the United States, Wallace and colleagues[29–31] introduced “Lymphoseek,” which consists of a dextran backbone covalently bonded to mannose units and linked to Tc-99m. The mannose units target the mannose-binding protein present on reticuloendothelial cells (phagocytic cells, such as macrophages) found in lymph nodes. The success rate of SLNM following intradermal and subcutaneous administration of Lymphoseek has been mixed, and further clinical trials are required to demonstrate improved injection site clearance and lymph node extraction as compared to Tc-99m-sulfur colloid.

In clinical practice, if a sentinel lymph node is found to be positive for tumor cells, then further lymph node dissection is typically performed to acquire adequate information for prognosis. In women with advanced cancer, complete axillary lymph node dissection (ALND) may also be performed. As a consequence of these lymph node dissections, 5–80% of the breast cancer patients undergoing SLNM and ALND develop breast cancer–related lymphedema (BCRL) in the arm.[32] To reduce this occurrence, Thompson *et al.*[33] recently proposed a novel technique of axillary reverse-mapping (ARM) that seeks to identify and preserve the lymphatics that drain the arm as opposed to those that drain the breast. In their study, 40 breast cancer patients who were scheduled for ALND and/or SLNM were injected with 37 MBq (1 mCi) of unfiltered Tc-99m sulfur colloid in 4 mL within the subareolar plexus for sentinel lymph node detection and 2.5 mL of blue dye subcutaneously or intradermally within the inner upper arm to map arm lymphatic drainage. In all patients, 100% of the resected sentinel lymph nodes were radioactive but not blue. In addition, pathologic examination revealed the negative status of the blue lymph nodes that drained the arm in the seven patients who had positive axillary lymph nodes. ARM may be an effective technique to prevent resection of arm lymphatics and subsequent occurrence of BCRL. However, a long-term prospective study is needed to ensure that along with a reduction in the risk of BCRL, the addition of ARM does not lower the accuracy of nodal staging.

Lymphoscintigraphy is also used to diagnose lymphedema and to assess lymphedema treatment efficacy on the basis of radiocolloid clearance rates, dermal backflow, and ratios of radioactivity in affected and unaffected regions. To investigate the potential of lymphoscintigraphy to evaluate lymphedema and to monitor response to therapy, Szuba *et al.*[32] administered 0.2 mL of 0.25 mCi Tc-99m filtered sulfur colloid subcutaneously in the first and second interdigital space of postmastectomy lymphedema patients. Figure 4 depicts a lymphoscintigram of a postmastectomy lymphedema patient with dermal backflow in the affected arm. Scintigraphy enabled quantitative estimation of dermal backflow and radioactivity ratio in the axilla of the affected arm to that in the healthy arm. In addition, the authors developed an empirical scoring system for postmastectomy lymphedema based upon visualization of lymph nodes and dermal backflow. Their results showed correlations of both the radioactivity ratio in the axilla of the affected arm to that in the healthy arm and the percent reduction in edema post treatment to both the lymphoscintigraphic score and excess initial arm volume. These results demonstrate the utility of lymphoscintigraphy to assess BCRL. Because the incidence of BCRL and the time at which the condition strikes varies from patient to patient, O'Mahony[34] and co-workers designed a lymphoscintigraphic study to identify lymphatic functional and morphologic changes in 19 patients who had undergone ALND. The authors performed intradermal injections of 0.1 mL of soluble Tc-99m human immunoglobin (40 MBq) in the second interdigital space of the hand to trace protein kinetics. Their rationale was that Tc-99m human immunoglobin is more stable than Tc-99m human serum albumin, has a slower blood clearance rate, and can provide information of lymphatic transport from its accumulation in blood. Although lymphatic architecture may be expected to change after ALND, there was a general tendency of more rapid appearance of radiolabeled proteins within the vascular space in patients who had undergone surgery than in those who had not. However, soluble radioisotopes such as Tc-99m human immunoglobin and Tc-99m human serum albumin may clear from injection sites by resorption into blood capillaries as well as by transport through the lymphatics. In order to link incidence of BCRL to more rapid appearance of protein in the bloodstream, a better understanding of the mechanism of transport from interstitium to the circulatory system is needed.

In addition to studies that involve interstitial injections to assess lymphedema, Peer *et al.*[35] recently reported on the use of intravenous injections of soluble Tc-99m hexakis-2-methoxy isobutyl isonitrile (Tc-99m MIBI) to detect AIDS-related cutaneous/subcutaneous Kaposi's sarcoma (KS) lesions and the associated condition of lymphadenopathy. KS is thought to arise from the vascular and lymphatic endothelium, and there are cases which report lymphadenopathy, and associated lymphedema can arise without the appearance of cutaneous/subcutaneous lesions. In these investigators' studies, the lymphoscintigrams of patients injected with 740 MBq (20 mCi) of Tc-99m MIBI showed accumulation in KS lesions and enabled detection of abnormal lymph nodes, suggesting its use for KS staging and for assessing response to therapy.

Lymphoscintigraphy has also been employed to assess the efficacy of emerging therapies for treatment of lymphedema. In order to investigate the success of transplanted autologous lymphatic vessels in patients with secondary lymphedema, Weiss *et al.*[36] conducted preoperative baseline and 8-year postoperative follow-up lymphoscintigraphy studies. To map the lymphatics of the affected limb, patients were given approximately 74 MBq (2 mCi) of Tc-99m nanocolloid injected subcutaneously into the first interdigital space. Lymphoscintigraphy scans provided lymph drainage maps that assisted in the planning of microsurgical interventions. Postoperative scintigraphy studies successfully depicted significant improvement of lymph drainage and visualization of lymph nodes. Thus, lymphoscintigraphy proved the potential of autologous lymph vessel transplant as a therapeutic option to treat lymphatic obstruction in lymphedema.[36,37] The recent discovery of lymphangiogenesis-inducing growth factor, VEGF-C (vascular endothelial growth factor

C), has provided another possible avenue to treat lymphedema. Administration of VEGF-C in the mouse skin[38] and rabbit ear[39] model of postsurgical lymphatic insufficiency has been shown to induce lymph vessel growth. However, the function of regenerating lymphatics is still unknown. In order to understand the physiology of regenerating lymphatics in an experimental animal model, Blacker and co-workers[6] employed lymphoscintigraphy after subdermal injections of 1.5 MBq in 10 μL of Tc-99m antimony trisulfide colloid (Tc-99m ATC) (~10 nm diameter), Tc-99m tin fluoride colloid (Tc-99mTFC) (~2000 nm diameter), and water-soluble, Tc-99m diethylenetriaminepentaacetic acid (Tc-99m DTPA) in order to examine depot clearance rates and lymph velocity in Australian geckos with original tails (OTs), fully regenerated tails (FRTs), and regenerating tails (RTs) at 6, 9, and 12 weeks after autotomy. Tc-99m ATC had a greater clearance and faster lymph velocity in OT geckos than in RT geckos. However, Tc-99m TFC had better clearance and faster velocity in RT than in FRT or OT animals, implying that larger particles were impeded as tail regeneration progressed. Last, water-soluble molecules immediately cleared from the injection site via venous capillaries in all tails, indicating that the slower clearance of colloids occurred via the lymphatics. The variable transit patterns for different types of radiopharmaceutical agents imply possible changes in vessel density and tissue porosity in the regenerating lymphatic model.

In summary, lymphoscintigraphy is a radionuclide-based imaging technique that enables two-dimensional visualization of the lymphatic network in cancer patients for lymph node staging and in lymphedema patients for evaluating response to therapy. Colloidal particle size and route of administration have an impact on the distribution of radiopharmaceuticals and the capacity for lymphatic imaging. For example, the imaging of lymphatic vessels was better enabled in BCRL patients by intradermal administration of Tc-99m human immunoglobin than subcutaneous administration because of the direct access to initial dermal lymphatics.[40] Nonetheless, the clinical evaluation of lymphedema remains qualitative or semiquantitative on the basis of clearance rates and dermal backflow parameters obtained from lymphoscintigraphy. Gamma camera integration times are typically long, preventing the dynamic imaging needed to quantitatively assess lymph flow, which, as we have found, is an inherent characteristic of healthy lymph vessels.

Positron Emission Tomography—Because of long gamma camera integration times, three-dimensional SPECT has not made a significant impact upon lymphatic imaging, whereas three-dimensional PET imaging promises to improve nodal staging in some kinds of cancer. PET involves intravenous injection of positron-emitting molecularly targeted radiopharmaceuticals to monitor biological processes and has been used to detect diseased lymph nodes.[30,41,42] PET images are often combined with X-ray CT to gain the additional advantage of structural information.[42] The contrast agents are typically analogues of naturally existing compounds or targeting agents that are either (1) isotopically substituted with a beta-emitting isotope (e.g., C-11,[43] N-13,[44] O-15,[45], F-18, I-124, I-125, or I-131)[30,42,43,46] or (2) conjugated to a chelating unit for sequestration of a beta-emitting substance, such as Cu-64 or Cu-61. 18-F-fluoro-2-deoxy-D-glucose (FDG) is the most common PET agent currently employed in the clinic. FDG is a glucose analogue with an –OH group replaced with F-18. The molecule is taken up by cells via Glut-1 transporter and, as in the case of glucose, undergoes phosphorylation to FDG-6-phophate, reflecting the hexokinase enzyme activity that is a rate-limiting step in glucose metabolism. However, FDG-6-phosphate is not further metabolically processed and becomes trapped within the cell. Since tumor cells exhibit increased glucose metabolism partly because of increased levels of glucose transporters and hexokinase enzyme activity, FDG-PET imaging may provide a means to localize sites of increased glucose metabolism, as in the case of reactive or cancer-positive lymph nodes.

PET has high sensitivity with a potential of signal detection at picomolar tissue concentrations of tracer, but falls short of conventional imaging techniques in terms of spatial resolution (~2 mm). A combination of the complementary roles of functional imaging by PET and anatomic imaging by CT has improved staging of malignancies.[14,47] Figure 5 depicts a sagittal CT scan (A), PET scan (B), and a coregistered PET-CT scan (C) of a patient with non–small cell lung cancer after intravenous injection of 350–400 MBq of FDG.[48] No enlarged lymph nodes are identified on the unenhanced CT scan. The PET scan identifies an area of increased FDG uptake, but it is difficult to identify the precise anatomic location of the abnormality. Integrated PET-CT, however, enables identification of a normally sized supraclavicular lymph node that was later excised and histologically confirmed for metastasis.[48] While 18-FDG PET-CT has been proposed to improve the diagnostic accuracy in nodal staging, not all kinds of cancer have higher glucose metabolism. Hence specificity and sensitivity for cancer nodal staging may prevent 18-FDG PET-CT from ubiquitous clinical use. However, more tumor-specific nuclear imaging agents are under development to more accurately perform nodal staging with PET.

Magnetic Resonance Imaging

Unlike nuclear imaging techniques, MRI is a technique that does not involve exposure to ionizing radiation. MRI utilizes magnetic properties of nuclei containing an odd number of protons and/or neutrons (such as the hydrogen atom) and their interaction with an external magnetic field and radiofrequency pulse to generate high-resolution images of the human body. T1-weighted images result from the relaxation of excited nuclei due to energy exchange with its surroundings, while T2 relaxation occurs from the exchange of energy between nuclei. MR lymphangiography involves interstitial or intravenous injection of contrast agents including gadolinium-labeled diethylene-triaminepentaacetic acid (Gd-DTPA), Gd dendrimers or liposomes, and iron oxide particles[14,49,50]

Pan and co-workers[51] demonstrated the feasibility of MR lymphangiography to assess lymphatic obstruction in the murine model of surgically induced tail lymphedema. T1-weighted MRI scans were conducted in normal and lymphedematous mice after subcutaneous tail injections of 0.1 mmol/kg Gd-DTPA 5 cm distal to the base of the tail. Unlike the normal mice, in which the two major bilateral collecting lymph vessels were visible from Gd-DTPA contrast (before rapid clearance), the lymphedematous mice showed accumulation of Gd tracer in the surgical site in the tail (1.6 cm distal from the base of the tail). In addition, lymph flow obstruction was assessed by comparing the mean signal intensity as a function of time in normal and edematous tails. Reduction in signal intensity with time at a region of interest (ROI) provided a measure of agent clearance in normal mice as opposed to the increase in signal intensity that indicated agent accumulation in edematous mice. These results demonstrate the feasibility of MR lymphangiography to assess lymphedema in experimental models. In human studies, Ruehm and co-workers[52] evaluated the potential of gadoterate meglumine, an extracellular paramagnetic agent, as an interstitial agent for visualization of lymphatics and lymph nodes in five healthy volunteers and three patients suffering from lymphatic disorders. After a total of 4.5 mL of contrast agent was injected into the dorsum of the foot, lymph vessels and lymph nodes could be clearly visualized from MR (indirect) lymphangiography. Lohrmann and colleagues[53–55] demonstrated the feasibility of detecting lymphatic vessels in patients with lymphedema using gadodiamide or gadoteridol, which are nonionic water-soluble paramagnetic contrast agents. A total amount of 4.5 mL of gadodiamide or 9 mL of gadoteridol at a dose of 0.1 mmol/kg of body weight was administered intracutaneously into the dorsal aspect of foot in the four interdigital spaces and medial to both first proximal phalanges. MR lymphangiography depicted lymphatic vessels, collateral vessels with dermal backflow, and inguinal lymph nodes. Figure 6 depicts enlarged lymphatic vessels (small arrows), dermal

backflow (arrowheads), and concomitantly enhanced veins (large arrow) in the left lower part of the leg of a 69-year-old man with primary lymphedema. The image was acquired 35 min after gadodiamide administration. Inguinal lymph nodes with external iliac lymphatics were also visualized in these studies. Recently, Matsushima *et al.*[56] reported unenhanced noninvasive visualization of the lymphatics of the trunk that included the thoracic duct, cisterna chyli, and lumbar lymphatics. In their studies, they employed heavily T2-weighted imaging with the addition of respiratory triggering to enable imaging of lymph separately from venous flows. Figures 7A to C depict coronal maximum intensity projection images of a 28-year-old male, with arrows identifying the cisterna chyli, and arrowheads indicating lumbar lymphatics and para-aortic lymphatic trunks. While other slowly flowing fluids may contaminate the images, the opportunity to assess lymphatic architecture without the administration of a contrast agent could have a significant impact on how we diagnostically assess the lymphatics.

The MRI techniques described above do not enable cancer staging of lymph nodes. MRI with super-paramagnetic iron oxide contrast may depict salient features of normal and cancer-positive lymph nodes.[53] Superparamagnetic contrast agents are composed of a water-insoluble crystalline magnetic core (4–6 nm in diameter), usually magnetite (Fe_3O_4) or magnemite (γ-Fe_2O_3), surrounded by a layer of dextran or starch derivatives. The particles shorten proton relaxation times, giving a signal distinct from tissue without particles. To detect diseased lymph nodes, dextran-coated ultra-small superparamagnetic iron oxide (USPIO) particles of less than 50 nm in diameter, known as ferumoxtran, have been intravenously injected into patients in investigational studies.[7] USPIO particles disseminate to lymph nodes via two mechanisms: (*a*) direct transcapillary migration across blood capillaries into the medullary sinuses within the lymph node; and (*b*) extravasation from the venules into the interstitium for uptake by lymph vessels draining to lymph nodes. The iron oxide particles may be subsequently phagocytosed by macrophages within the lymph nodes, introducing field inhomogeneities that reduces signal. Bellin *et al.*[57] studied the uptake of USPIO particles in normal and diseased lymph nodes. The observed T2-weighted images in Figure 8 show inhomogeneities in benign lymph nodes, which are produced by accumulated iron oxide particles. Figure 8A depicts a precontrast image of external iliac lymph nodes of a patient with prostate cancer. The arrows indicate iliac lymph nodes that have high signal intensity. Figure 8B depicts the image of normal iliac lymph nodes (arrows) acquired after injection of 1.7 Fe/kg USPIO that appear to be dark on account of agent accumulation. Malignant lymph nodes that lack reticuloendothelial cells cannot accumulate USPIO and thus retain the bright MR signal.[14,57,58]

The high spatial resolution of MRI has the greatest potential for assessing the morphology of the lymphatic system, including lymph vessels and nodes. USPIOs provide indirect evidence of nodal cancer involvement through negative contrast and until sensitivity and specificity for nodal detection can be determined it is unlikely that they will supplant current biopsy procedures. While enhanced MR lymphangiography shows great promise for limb imaging, the opportunity for unenhanced lymphangiography for imaging the lymphatic tract holds unprecedented promise for diagnosis and treatment planning of lymphatic disorders.

Ultrasound

US employs sound waves at frequencies ranging from 1 MHz to 20 MHz (or 1.57 mm to 0.08 mm in wavelengths within tissue) that exceed the frequency range audible to humans. The US device consists of a transducer that emits US waves that pass through tissue and, upon encountering tissues of varying acoustic properties, generate echoes that are registered by piezodetectors placed at the tissue surface.[59] US is the imaging modality most frequently used for evaluation of a parasitic form of lymphedema called *filariasis*. Suresh *et al.*[60] reported the use of US to detect dilated lymph vessels in patients with filariasis as well as to

measure worm motion within lymphatics using Doppler US. Used typically to quantify the velocity of blood flow toward and away from a US probe, Doppler US is unable to assess acellular lymph flow. However, Mellor *et al.*[61] reported the use of Doppler US to examine venous flow of patients with lymphedema–distichiasis (LD) who had known mutations in the *FOXC2* gene. While FOXC2 mutations are implicated in defective lymphatic valves, Mellor and co-workers found venous reflux and venous valvular incompetence in the proximal veins in LD patients. The result may not be surprising considering the close genetic relationship between lymphatic and hemovascular disorders and that many of the venous vasculopathologies clinically evaluated may also have an unidentified lymphatic component.

In addition to lymphedema, US may be utilized to characterize metastatic lymph nodes on the basis of their size, shape, and echogenicity using US. A US image of a normal lymph node appears ellipsoid in shape, with hypoechoic cortex and hyperechoic hilum. A malignant lymph node can appear round with loss of hyperechoic hilum and noticeable hypoechogenicity of cortex.[14] Since it does not employ a contrast agent, US imaging of lymph nodes may prove to be useful for detecting tumor burden in lymph nodes that obstruct the drainage of radiotracer to sentinel lymph nodes, thereby providing false negative SLNM results. While nodal staging by ultrasonography is reported to have sensitivity ranging from 50% to 87%,[62,63] and specificity of up to 92%[62]; and the addition of fine-needle aspiration is reported to have a controversial sensitivity ranging from 18% to 78.5% and specificity of 93.5%–100%,[62,63] it is unlikely that US can detect occult micrometastases, which are increasingly thought to be clinically relevant. US is also restricted from studying deep lymph nodes.

Contrast-enhanced ultrasonography includes the administration of submicron-sized microbubbles to image the microcirculation as well as the lymphatics and lymph nodes in animals.[13,49,64,65] The echogenic microbubbles are phagocytosed by macrophages or reticuloendothelial cells and appear bright on an ultrasonogram. Malignant lymph nodes that lack reticuloendothelial cells cannot take up the microbubbles and remain hypoechoic. Goldberg *et al.*[65] injected a milliliter volume of 2.4–3.5 μm diameter, lipid-stabilized perflurobutane microbubbles subcutaneously or intradermally in the peritumoral region of swine. Figures 9A and B illustrate US scans of a normal lymph node at pre- and postcontrast in a swine model of melanoma. The postcontrast US scans depict hyperechoic lymph nodes. Figure 9C represents a contrast-enhanced lymphatic channel draining into a sentinel lymph node (N) after an intradermal injection of microbubbles. Last, Figure 9D indicates a post-contrast US scan of a lymph node (arrows), mostly composed of hypoechoic region depicting buildup of melanoma tumor cells (T), with a small region of normal tissue (N) that demonstrates contrast enhancement. Hauff and co-workers[66] developed and utilized L-selectin ligand-specific polymer-stabilized air-filled microparticles (MPs) for active targeting of peripheral lymph nodes in mice and dogs. The feasibility of detecting lymph nodes by molecularly targeting the L-selectin ligand present on high endothelial venules was demonstrated by intravenous injection of MPs (10–14 million particles per kg) in mice or dogs by means of stimulated acoustic emission (SAE) ultrasonography, in which the applied US caused bursting of microbubbles and generation of harmonic US frequencies for detection. The technique provides yet another potential tool to detect cancer-positive lymph nodes with specificity depending upon the targeting, which in this case was a nonspecific L-selectin ligand in a cancerous node. Unfortunately, the microbubble agent is destroyed in the process of SAE imaging.

Optical Imaging

Optical imaging is based upon the administration of contrast agents that, when excited by tissue propagating excitation light, exhibit fluorescence. The process of fluorescent emission

occurs when an incident photon of resonant energy is absorbed by a molecule residing at equilibrium in a ground state. The molecule, upon absorption of the photon, is subsequently excited to a higher electronic energy level. Fluorescence occurs when the molecule radiatively relaxes, releasing the energy required for it to return back to its ground state. The energy released is in the form of photons that either have wavelengths in the visible range (400–700 nm) or in the NIR region (700–900 nm). Blood, melanin, and water have a low absorption of light in the NIR region[67] that enables NIR light to penetrate deeply in tissues.

Fluorescence microlymphangiography utilizes contrast agents, such as fluorescein, which is excited and emits at visible wavelengths and, as a result, provides information on superficial lymphatics. The technique utilizes interstitial injections of approximately 10 μL of fluorescein isothiocyanate dextran and 494-nm excitation illumination of the superficial lymphatics.[68,69] Figure 10 compares fluorescence microlymphangiograms after the administration of 10 μL of 25% (w/v) fluorescein isothiocyanate into the dermis on the ventral aspect of the normal (panel A) and affected forearm (panel B) of a BCRL patient. The superficial fluorescent lymphatic channels are visualized by fluorescent video microscopy usually across a quarter-sized area, and demonstrate the denser lymphatic network in the dermis of the edematous as opposed to the unaffected arm. In addition to mapping the superficial lymphatics, microlymphangiography may enable noninvasive estimation of the width of lymph channels.[69] Fluorescence imaging of lymph nodes in the visible wavelength range was also demonstrated by McGreevy *et al.*,[70] who utilized a contrast agent that was constituted of a red fluorescent dye, Cy5, conjugated to vitamin B_{12} for excitation at 633–650 nm and emission at 668 nm. Increased sequestration of cobalamin (vitamin B_{12}) by primary tumor cells is hypothesized to provide contrast for cancer-positive lymph nodes. Its feasibility to detect lymph nodes was demonstrated in normal swine following intradermal injection of 1 mL containing 1.5 mg of the conjugate. However, because of the limited tissue penetration depth of the visible light, the investigators were not able to image deep lymphatics, such as pre- and postcollector vessels.

The NIR emission from quantum dots (QDs) offers somewhat better tissue penetration, but QDs are mostly excited by visible light and are restricted from deep tissue imaging. Type II core/shell QDs are semiconductor nanocrystals that can comprise of a core of cadmium telluride, a shell of cadmium selenide, and an outer coating of soluble phosphines.[71] QDs have a hydrodynamic diameter of 15–20 nm and a peak emission of 840 nm.[71] Injections of type II QDs within the footpad of rodents,[72] the intraparenchymal[73,74] and submucosal esophageal[71,73] spaces, have demonstrated the feasibility of intraoperative mapping of lymph nodes for resection and subsequent biopsy. Even though the use of high quantum yield type II QDs enables visualization of lymph nodes reportedly as deep as 1 cm within an intraoperative field, concerns about the fate and toxicity of QDs due to their heavy metal content may impede their translation into the clinic.

NIR imaging involves intradermal, subcutaneous, or intravenous injections of fluorescently labeled soluble agents to map lymphatic vasculature. Previously, Gurfinkel *et al.*[75] reported the use of intravenous injections of 1.0 mg kg^{-1} of an NIR dye, indocyanine green (IC-Green), for excitation at 778 nm and collection of emission at 830 nm and 0.3 mg kg^{-1} of carotene-conjugated 2-devinyl-2-(1-hexyloxyethyl) pyropheophorbide (HPPH-car) with excitation at 660 nm and collection of fluorescence at 710 nm to image reactive lymph nodes within a canine population with spontaneous mammary disease. HPPH-car is a photodynamic agent modified with a carotene moiety to eliminate the cytotoxic triplet state upon excitation. Unfortunately, the suboptimal red excitation and emission of HPPH-car restricted the tissue penetration of both excitation and emission light in comparison to the NIR dye, IC-Green. Recently, Sharma and co-workers[76] reported quantitative optical imaging of lymph function in anesthetized swine after intradermal injections of about 200

μL of 3–32-μM IC-Green and showed for the first time, dynamic lymph propulsion of "packets" that traveled on the order of 0.1–1 cm/s. The unique opportunities enabling dynamic fluorescent imaging and emerging results in humans are described in more detail below. However, prior to this work, lymph flow was reported in animal preparations to be on the order of μm/s,[77] instead of the cm/s that was quantitatively and noninvasively imaged using NIR optical imaging.

NIR optical imaging technique has also been employed for mapping lymphatics in humans. Kitai *et al.*[78] and Motomura *et al.*[79] demonstrated mapping of lymphatic trunks after subdermal administration of 25 mg of IC-Green. Kitai *et al.*[78] used fluorescence, while Motomura *et al.*[79] visually tracked the green dye. In addition, Unno and co-workers[80] used fluorescence from IC-Green to map lymphatics of secondary lymphedema patients and healthy subjects. Subcutaneous injections of 1 mg IC-Green in the dorsum of the foot of lymphedema patients depicted dilated lymph channels, dermal backflow, and accumulation of dye in the dorsal and plantar region of the foot as opposed to discrete lymphatic channels in healthy subjects. Recently, Sevick-Muraca *et al.*[81] reported the results from quantitative optical imaging of lymph flow in breast cancer patients following microdose (i.e., less than 100 μg) administration of IC-Green. The first report of optical lymph imaging in humans at trace amounts of IC-Green demonstrates the potential to administer an NIR-labeled, targeting contrast agent for the noninvasive nodal staging of cancer-positive lymph nodes as proposed by Sampath *et al.*[82]

Unique Opportunities for Imaging Lymphatic Function

Evaluation of functional status of lymph channels will be crucial for developing an understanding of lymphatic biology, evaluating the role of the lymphatics in health and disease, as well as diagnosing patients with disorders of the lymphatic system. Once a quantifiable imaging approach for assessing lymphatic function is developed and made available for clinical study, the opportunity to assess new therapeutic strategies and pharmacologic agents may spur the development of new treatments for patients suffering from lymphatic disorders. Fortunately for lymphatic imaging, NIR technology may be simple and economic to employ. As detailed below, NIR fluorescence imaging represents the only imaging modality to date sensitive enough for the direct imaging of propulsive lymph flow through lymphatic vessels deep within tissues.

The reason for the sensitivity arises from the penetration of NIR light, optimally in the wavelength range of 750–850 nm, and the ability to stably and repeatedly re-activate NIR-excitable dyes. To illustrate the sensitivity, compare a radiotracer (whether a gamma- or positron-emitter for the nuclear imaging techniques described above) and a typical NIR fluorophore. Whether produced in a cyclotron or generator, a radiotracer relaxes only once, emitting a single photon event before becoming spent. On the other hand, once a stable NIR fluorophore relaxes in tissues generating a fluorescent photon, it can be subsequently reactivated by propagating excitation light, enabling it to relax multiple times. Since the lifetime, or the mean time that the fluorophore resides in its activated state, is on the order of a nanosecond, theoretically there can be as many as one billion fluorescent photons emitted from a single fluorescent molecule per second. Realistically, low quantum efficiencies for fluorescent photon generation, high tissue attenuation of propagating excitation and emission photons, and other instrumentation factors prevent such enormous fluorescent photon output. Nonetheless, in a study of a dual-labeled NIR optical and gamma-emitter, Houston and co-workers[83] found that the image quality of NIR optical imaging surpasses gamma scintigraphy in small animals, even though NIR imaging required only 800 ms of integration time while gamma scintigraphy required 15 min.

It is the high sensitivity of NIR optical imaging that allows image integration times to range from 50 ms to 800 ms, enabling rapid pharmacokinetic analysis of dye uptake[75,84] from images as well as imaging of lymph trafficking. While pulsatile lymph flow has been quantified using intravital microscopy techniques in the mesentery of animals, there have been no previous reports of quantifiable lymphatic flow from non-invasive imaging. More recently, the ability to optically image propulsive lymph flow in swine,[76] mice,[84] and humans[81] has been demonstrated. The common feature in these studies is the use of an image-intensifier which is sensitive in the NIR wavelength range, and a frame-transfer, 16-bit CCD camera which enables rapid and sensitive data acquisition with a low noise floor. The noise floor of fluorescence optical image acquisition arises because of autofluorescence as well as excitation light leakage through the rejection filters, which enable selective passage of fluorescent light to the image intensifier. For NIR imaging, the autofluorescence is virtually zero, but as one moves into the red excitation wavelengths using red exciting dyes, natural porphyrins and chlorophylls (from food) create a background that can obscure the signal from the fluorophore. In addition, the use of holographic rejection filters, which block 10 orders of magnitude of collimated, monochromatic excitation light, can also reduce the noise floor. Unfortunately, few commercially available instruments for small-animal imaging employ holographic filters. In addition, the success of holographic filters depends upon collimating the incident light and removing all possible stray light components. Not widely recognized is the fact that the use of broadband excitation sources, such as light-emitting diodes and lamps, reduce the effectiveness of holographic and interference filters, since these light sources are seldom monochromatic enough for effective blockage of excitation light. Finally, the availability of NIR-excitable dyes has increased in the past few years. IC-Green is approved in humans for assessing cardiac and hepatic function and for ophthalmologic studies and can be excited serendipitously at 780 nm, with a significant Stoke's shift enabling fluorescent measurement at 830 nm and greater. Small Stoke's shifts less than 30–40 nm can cause significant problems as they impede the ability to efficiently reject excitation light and collect the fluorescent signal. Unfortunately, IC-Green does not have a functional group and cannot be conjugated with a targeting peptide, protein, polysaccharide, or other molecule, but it can be used as a soluble dye which noncovalently associates with albumin to create a lymphotropic agent. A few commercially available NIR-excitable dyes with functional groups for creating molecular imaging agents are now available with sufficient Stoke's shifts: IRDye800 CW (Licor, Inc., Lincoln NE), AlexaFluor 790 (Invitrogen, Carlsbad, CA), and Cy7 and Cy 7.5 (Amersham/GE Health-Science, Piscataway, NJ). Usually, as a general rule of thumb, it is important to excite NIR organic dyes with as narrow or as monochromatic source as possible in order to maximally reflect excitation light, and to use bandpass filters well away from the excitation line in order to collect as much emission as possible for enhanced sensitivity. With these caveats, as shown below, the use of NIR optical imaging of lymphatic function offers a new, economical, and significant research and diagnostic tool to the lymphatic research community. In the following, we briefly review the progress in dynamic imaging of lymphatic function in mice, swine, and humans as well as highlight the opportunities and challenges specific to each.

Lymph Imaging in Mice

Preclinical investigation of potential pro- and anti-lymphangiogenic agents are typically performed in rodent models, thereby necessitating the imaging of lymphatic function in these small-animal models. While their small size may facilitate imaging, the temporal and spatial resolution provides challenges for functional lymphatic imaging in small animals. As comprehensively reviewed by Kwon and Sevick-Muraca,[84] lymphatic vessels in mice and rats have been imaged using (1) radiography to visualize mercury uptake in the two major lymph vessels in the mouse tail,[85] and (2) micro-MR lymphangiography with Gd-laden

dendrimers[86–88] and (3) fluorescence video-microscopy to see the circumferential "honeycomb" lymphatic structure in the mouse tail.[89–91] Lymphatic function has also been inferred from lymphoscintigraphy and microangiography by Slavin *et al.*,[92] who reported that myocutaneous flap transfer restores lymphatic function. Several groups have demonstrated lymphatic transport of QDs to map out drainage patterns.[72,93,94] Wunderbaldinger *et al.*[95] used an enzyme-sensing optical probe with visible wavelength excited fluorophore, Cy5.5, for the detection of lymph nodes. To date there have been few, if any, studies that demonstrated contractile lymphatic motion that characterizes lymphatic function in larger animals. As shown in Figure 11, Kwon and Sevick-Muraca[84] recently demonstrated the ability to image IC-Green trafficking from the lymph plexus, through lymph vessels and lymphangions, to ischial nodes in the tail and to axillary nodes in mice. The intensity profile shows that the peak fluorescence occurs at an average of every 6.56 ± 1.14 s and the lymph flow velocity ranged from 0.28 mm/s to –1.35 mm/s. Lymph flow velocities from the propelled IC-Green packet in the major lymph vessels in the mouse tail ranged from 1.33 mm/s to –3.88 mm/s. While pulsatile lymph flow was detected in the deep lymph vessels, lymph propulsion was not visualized in the superficial lymphatic network of the tail. When imaging lymph flow to the axillary nodes, propulsive lymph flow was also detected.

The ability to image contractile motion in mice provides new opportunities to (1) assess lymphatic function in transgenic mice models to better understand the role that specific gene expression has on the lymphatic function and to (2) investigate pharmacologic agents that stimulate the formation of functional lymphatics as well as stimulate the contractile apparatus of existing lymphatics.

Lymph Imaging in Swine

Yorkshire swine is the commonly preferred animal model for preclinical lymph-imaging investigations, as swine skin and lymph drainage pattern are similar to those of human skin.[70,96] Similar to human dermis, swine dermis is characterized by open-ended lymphatic capillaries that take up particles and lymphotropic agents under a pressure gradient. Passively diffusing agents, such as soluble NIR fluorophores, are taken up in the initial lymphatics and then drain into afferent lymphatic channels that propel lymph to the lymph nodes. Recently, we reported results of quantitative imaging of afferent lymphatic function in swine.[76] In addition to mapping lymphatic vasculature after intradermal injections of 100–200 μL of 32-μM IC-Green near mammary teats or on hindlimb, we conducted quantitative analysis of (1) the lymph flow velocities of transiting "packets" of IC-Green, and (2) their frequency of propulsion caused by lymphangion contractions. The "packets" of dye transited along lymph vessels 2–16 cm in length at velocities of 2.3–7.5 mm/s and frequencies of 0.5–3.3 pulses per minute. Figure 12 illustrates pulsatile lymph flow in a swine lymphatic. The figure represents images of a bolus of IC-Green (circle) transiting along a swine's abdominal lymph channel from the injection site around the mammary teat to the inguinal lymph node at times 0, 2.6, and 5.2 s. The pulsatile lymph flow was also analyzed quantitatively to compute the period between the "packets" of dye transiting along a lymph channel. Figure 13 represents a plot of intensity profile at an ROI on an abdominal lymph channel as a function of imaging time after injection of 200 μL of 32-μM IC-Green around the mammary teats of swine. The peaks indicate a "bolus" of fluid transiting from the injection site to the inguinal lymph node on an average at every 72 s. Since manual lymphatic drainage (MLD) is an important component of complete decongestive therapy for lymphedema patients,[97] we employed the noninvasive lymph-imaging technique to measure the efficacy of MLD in a healthy anesthetized swine. For instance, in one case, the NIR optical lymph-imaging technique enabled detection of change in lymph flow velocity in a swine abdominal lymphatic from 6.2 (±1.9) mm/s to 8.0 (±2.5) mm/s and change in the

mean period between pulses from 48 (±37) to 69 (±40) s in response to massage. Noninvasive determination of pulsatile lymph flow and transport velocities via imaging can provide a tool to evaluate lymphatic function in response to existing therapies and may help assess function of newly regenerated lymph channels in response to novel therapeutic interventions, including VEGF-C or gene therapies.

Lymph Imaging in Humans

The preclinical imaging studies in swine demonstrated the feasibility of performing deep tissue lymph imaging with microgram quantities of IC-Green. To translate the technique to the clinic we take advantage of the established safety record of IC-Green given in mg quantities. Sevick-Muraca *et al.*[81] recently reported the feasibility of detecting sentinel lymph nodes with microgram administration of IC-Green in breast cancer patients. Figure 14A depicts a white-light and fluorescent image overlay of a 46-year-old African American breast cancer patient intradermally injected with 100 μL of 20 μg IC-Green in each quadrant of the peri-areolar region on her right breast. The injection sites were covered with an opaque plastic to prevent oversaturation of the imaging camera. Arrows indicate lymphatics pooling the dye to axilla. Figure 14B represents the pulsatile lymph flow in the breast lymphatics. The peaks in the plot of intensity profile at an ROI (oval in panel A) as a function of duration of image acquisition indicate that the lymph channel conducts “packets” of IC-Green from the injection site to the axilla on an average every 22.9 ± 7.8 s at a velocity of 2.2 (±0.6) mm/s. A fluorescent “hot-spot” in the axilla was resected and found to be a sentinel lymph node. IC-Green is now being used for human lymph imaging in an ongoing feasibility study to compare lymph flow of healthy subjects and lymphedema patients as next described.

Before aberrant lymphatic function can be identified through NIR imaging, baseline lymphatic function was first evaluated in healthy volunteers. Figure 15 shows white-light and fluorescent overlay images of a foot of a 46-year-old Caucasian female in a supine position during image acquisition. The subject was injected with 100 μL of 25 μg of IC-Green each in the first and second interdigital spaces (arrows) in the dorsum of the foot. The images are a combination of the white-light photograph of the foot overlain with corresponding fluorescent images at 0, 2, and 15 s. The circle identifies a “packet” of dye transiting at a velocity of 5.0 mm/s between lymphangions along the lymphatic channel, while the arrowheads identify the localized collection of fluorescent dye that demarks lymphangions. The period between two consecutive pulses observed during image acquisition was 164 s. Figure 16 is another white-light and fluorescent image overlay that illustrates the lymphatic vasculature of a human hand. The image represents a hand of a 22-year-old Caucasian male in a supine position at the time of imaging. The subject was injected with 100 μL of 25 μg of IC-Green in the four interdigital spaces. The velocity of a single packet transiting in one of the lymph vessels draining an injection site next to the thumb was 16.6 mm/s. The ability to safely and noninvasively map the lymphatic network, locate lymphangions, and quantify lymph function in healthy volunteers can be employed for a comparative assessment of lymph drainage in persons with lymphedema. In addition, the potential to detect pulsatile lymph flow noninvasively using microdose concentrations of IC-Green augurs well for molecular imaging of lymphatics.

Molecular Staining of Lymph Endothelium for Imaging Using Hyaluron

The sudden interest in lymphatic research is in part attributed to the discovery of lymph-specific biomarkers, such as Prox-1, podoplanin, and lymph endo thelial-specific hyaluronan receptor 7 (LYVE-1),[1] and regulators of lymphangiogenesis. Of these biomarkers, LYVE-1 is not only expressed on lymphatic endothelium, but is also found on liver sinusoids, tubular epithelial cells of kidney, cells from adrenal glands and pancreas, and tumor-infiltrating

macrophages.[98–100] The expression of LYVE-1 is correlated with poor prognosis of breast, endometrial, lung, and head and neck cancer,[101,102] and it is hypothesized that the kinds of cancer that have a tendency to metastasize express lymph markers. LYVE-1 is thought to mediate cell adhesion, uptake of hyaluronan (HA) from tissue for catabolism in lymph endothelial cells, and transport of HA from tissues to lymph across the lymphatic endothelium via transcytosis for its subsequent degradation in the nodes.[100,103,104] Hyaluron, an important component of the extracellular matrix, is an acidic glucosaminoglycan made of repeating disaccharides, and is synthesized by fibroblasts and other mesenchymal cells.[103–105] It is suggested that HA plays a key role in regulating interstitial hydration, plasma protein exclusion, maintaining interstitial fluid volume, supporting cell adhesion and migration in embryogenesis and wound healing, and in inducing inflammation.[103,106,107] While 90% of all HA is degraded in the lymph nodes, the remaining HA is subsequently taken up and broken down in the liver. HA is approved by Food and Drug Administration for use in joint therapy and correction of facial wrinkles.

Recently, we reported swine lymph vessel staining with an NIR dye conjugated to HA that binds to LYVE-1 on the lymphatic endothelium. Figure 17 depicts a plot of mean fluorescent intensity of an ROI identified on a swine leg lymph vessel stained with HA-NIR and IC-Green for dynamic imaging as a function of time. Figure 17A depicts an ROI selected on a leg lymph vessel stained with HA-NIR dye. Figure 17B represents an ROI selected on a leg lymph vessel with trafficking IC-Green. Figure 17C compares the intensity profiles in the two lymph vessels. The initial peaks of fluorescent intensity for IC-Green, a nonspecific dye, indicate that the dye is propelled as “packets” of fluid and cleared out of the lymph vessel. On the other hand, the fluorescence intensity due to HA-NIR remains almost unchanged for the duration of image acquisition. The observation supports the hypothesis that HA-NIR binds to LYVE-1 present on the lymph endothelium. Kitayama and colleagues[108] recently reported the use of free HA mixed with patent blue or ferumoxides to map sentinel lymph nodes in patients undergoing gastric cancer surgery. Submucosal injections of one part HA and four parts patent blue or ferumoxides resulted in long tracer retention times in the sentinel nodes (<2 h) as opposed to patent blue or ferumoxides alone, which stained the efferent lymphatics within 20 min. In summary, since HA is a ligand for LYVE-1 present on the lymph endothelium, NIR imaging agents conjugated to HA may enable accurate detection of sentinel lymph nodes in cancer patients and computation of lymphatic vessel architecture and density in patients with lymphatic disorders.

Summary

From the compendium of imaging techniques summarized above, one can see that new opportunities for imaging lymphatic architecture and function are promised primarily from the development of new imaging agents and perhaps by the emergence of fluorescent optical imaging technologies. The translation of these discoveries into clinical practice may first depend upon their successful demonstration in preclinical models of lymphatic impairment and repair. With the ultimate adoption of noninvasive imaging and novel imaging agents in the clinic, it may be possible to obtain more accurate phenotyping for identification of genetic bases of lymphatic disorders, furthering advanced understanding of human disease.

References

1. Alitalo K, Tammela T, Petrova TV. Lymphangiogenesis in development and human disease. Nature. 2005; 438:946–953. [PubMed: 16355212]
2. Baluk P, Tammela T, Ator E, et al. Pathogenesis of persistent lymphatic vessel hyperplasia in chronic airway inflammation. J Clin Invest. 2005; 115:247–257. [PubMed: 15668734]

3. Ji RC. Characteristics of lymphatic endothelial cells in physiological and pathological conditions. Histol Histopathol. 2005; 20:155–175. [PubMed: 15578435]
4. Harvey NL, Srinivasan RS, Dillard ME, et al. Lymphatic vascular defects promoted by Prox1 haploin-sufficiency cause adult-onset obesity. Nat Genet. 2005; 37:1072–1081. [PubMed: 16170315]
5. Cueni LN, Detmar M. New insights into the molecular control of the lymphatic vascular system and its role in disease. J Invest Dermatol. 2006; 126:2167–2177. [PubMed: 16983326]
6. Blacker HA, Tsopelas C, Orgeig S, et al. How regenerating lymphatics function: lessons from lizard tails. Anat Rec. 2007; 290:108–114.
7. Moghimi SM, Rajabi-Siahboomi AR. Advanced colloid-based systems for efficient delivery of drugs and diagnostic agents to the lymphatic tissues. Progress Biophys Mol Biol. 1996; 65:221–249.
8. Enderle, JD.; Blanchard, SM.; Bronzino, J. Introduction to Biomedical Engineering. Academic Press; San Diego, CA: 2000.
9. Hultén L, Åhrén C, Rosencrantz M. Lymphangio-adenography in carcinoma of the breast. Acta Chirurg Scand. 1966; 132:261–274.
10. Kinmonth JB. Lymphangiography in man; a method of outlining lymphatic trunks at operation. Clin Sci. 1952; 11:13–20. [PubMed: 14896514]
11. Kinmonth, JB. The Lymphatics: Diseases, Lymphography and Surgery. Edward Arnold; London: 1972.
12. Kos S, Haueisen H, Lachmund U, et al. Lymphangiography: forgotten tool or rising star in the diagnosis and therapy of postoperative lymphatic vessel leakage. Cardiovasc Intervent Radiol. 2007; 30:968–973. [PubMed: 17508245]
13. Witte CL, Witte MH, Unger EC, et al. Advances in imaging of lymph flow disorders. Radiographics. 2000; 20:1697–1719. [PubMed: 11112825]
14. Barrett T, Choyke PL, Kobayashi H. Imaging of lymphatic system: new horizons. Contrast Media Mol Imaging. 2006; 1:230–245. [PubMed: 17191764]
15. Silvestri RC, Huseby JS, Rughani I, et al. Respiratory-distress syndrome from lymphangiography contrast-medium. Am Rev Resp Dis. 1980; 122:543–549. [PubMed: 6254413]
16. Tiwari A, Cheung K-S, Button M, et al. Differential diagnosis, investigation, and current treatment of lower limb lymphedema. Arch Surg. 2003; 138:152–161. [PubMed: 12578410]
17. Vogl TJ, Bartjes M, Marzec K. Contrast-enhanced lymphography. CT or MR imaging? Acta Radiol Suppl. 1997; 412:47–50. [PubMed: 9240080]
18. Partsch H, Urbanek A, Wenzel-Hora B. The dermal lymphatics in lymphoedema visualized by indirect lymphography. Br J Dermatol. 1984; 110:431–438. [PubMed: 6712887]
19. Partsch H, Wenzel-Hora BI, Urbanek A. Differential diagnosis of lymphedema after indirect lymphography with Iotasul. Lymphology. 1983; 16:12–18. [PubMed: 6843172]
20. Pecking AP, Desprez-Curley JP, Cluzan RV. Tests and imaging of the lymphatic system. Rev Med Interne. 2002; 23:d391s–397s.
21. Suga K, Ogasawara N, Yuan Y, et al. Visualization of breast lymphatic pathways with an indirect computed tomography lymphography using a nonionic monometric contrast medium iopamidol: preliminary results. Invest Radiol. 2003; 38:73–84. [PubMed: 12544070]
22. Suga K, Shimizu K, Kawakami Y, et al. Lymphatic drainage from esophagogastric tract: feasibility of endoscopic CT lymphography for direct visualization of pathways. Radiology. 2005; 237:952–960. [PubMed: 16304114]
23. Wisner ER, Ferrara KW, Short RE, et al. Indirect computed tomography lymphography using iodinated nanoparticles to detect cancerous lymph nodes in a cutaneous melanoma model. Acad Radiol. 1996; 3:40–48. [PubMed: 8796639]
24. Rabin O, Perez JM, Grimm J, et al. An X-ray computed tomography imaging agent based on long circulating bismuth sulphide nanoparticles. Nat Mater. 2006; 5:118–122. [PubMed: 16444262]
25. Yuan Z, Chen L, Luo Q, et al. The role of radionuclide lymphoscintigraphy in extremity lymphedema. Ann Nucl Med. 2006; 20:341–344. [PubMed: 16878705]

26. McNeill GC, Witte MH, Witte CL, et al. Whole-body lymphangioscintigraphy: preferred method for initial assessment of the peripheral lymphatic system. Radiology. 1989; 172:495–502. [PubMed: 2748831]
27. Szuba A, Shin WS, Strauss HW, et al. The third circulation: radionuclide lymphoscintigraphy in the evaluation of lymphedema. J Nucl Med. 2003; 44:43–57. [PubMed: 12515876]
28. Sato T, Yamaguchi K, Morita Y, et al. Lymphoscintigraphy for the interpretation of changes of cervical lymph node function in patients with oral malignant tumors: comparison of Tc-99m-Re and Tc-99m-HSA-D. Oral Surg Oral Med Oral Pathol Oral Radiol Endod. 2000; 90:526–536.
29. Wallace AM, Hoh CK, Vera DR, et al. Lymphoseek: a molecular radiopharmaceutical for sentinel node detection. Ann Surg Oncol. 2003; 10:531–538. [PubMed: 12794019]
30. Schöder H, Glass EC, Pecking AP, et al. Molecular targeting of lymphovascular system for imaging and therapy. Cancer Metastasis Rev. 2006; 25:185–201. [PubMed: 16770532]
31. Ellner SJ, Hoh CK, Vera DR, et al. Dose-dependent biodistribution of [(99m)Tc]DTPA-mannosyl-dextran for breast cancer sentinel lymph node mapping. Nucl Med Biol. 2003; 30:805–810. [PubMed: 14698783]
32. Szuba A, Strauss W, Sirsikar SK, et al. Quantitative radionuclide lymphoscintigraphy predicts outcome of manual lymphatic therapy in breast cancer-related lymphedema of the upper extremity. Nucl Med Commun. 2002; 23:1171–1175. [PubMed: 12464781]
33. Thompson M, Korourian S, Henry-Tillman R, et al. Axillary reverse mapping (ARM): a new concept to identify and enhance lymphatic preservation. Ann Surg Oncol. 2007; 14:1890–1895. [PubMed: 17479341]
34. O'mahony S, Bennett Britton TM, Solanki CK, et al. Lymphatic transfer studies with immunoglobin scintigraphy after axillary surgery. Eur J Surg Oncol. 2007; 33:1052–1060. [PubMed: 17499475]
35. Peer FI, Puri MH, Mosam A, et al. 99mTc-MIBI imaging of cutaneous AIDS-associated Kaposi's sarcoma. Int J Dermatol. 2007; 46:166–171. [PubMed: 17269969]
36. Weiss M, Baumeister RJH, Hahn K. Post-therapeutic lymphedema: scintigraphy before and after autologous lymph vessel transplantation 8 years of long-term follow-up. Clin Nucl Med. 2002; 27:788–792. [PubMed: 12394126]
37. Weiss M, Baumeister R, Hahn K. Dynamic lymph flow imaging in patients with oedema of the lower limb for evaluation of the functional outcome after autologous lymph vessel transplantation: an 8-year follow-up study. Eur J Nucl Med Mol Imaging. 2003; 30:202–206. [PubMed: 12552337]
38. Saaristo A, Tammela T, Timonen J, et al. Vascular endothelial growth factor-C gene therapy restores lymphatic flow across incision wounds. FASEB J. 2004; 18:1707–9. [PubMed: 15361472]
39. Szuba A, Skobe M, Karkkainen MJ, et al. Therapeutic lymphangiogenesis with human recombinant VEGF-C. FASEB J. 2002; 16:1985–1987. [PubMed: 12397087]
40. O'Mahony S, Solanki CK, Barber RW, et al. Imaging of lymphatic vessel in breast cancer related lymphedema: intradermal versus subcutaneous injection of 99mTc-immunoglobulin. Am J Roentgenol. 2006; 186:1349–1355. [PubMed: 16632730]
41. Delbeke D. Oncological applications of FDG PET imaging: brain tumors, colorectal cancer lymphoma and melanoma. J Nucl Med. 1999; 40:591–603. [PubMed: 10210218]
42. Hoffman JM, Gambhir SS. Molecular imaging: the vision and opportunity for radiology in the future. Radiology. 2007; 244:39–47. [PubMed: 17507723]
43. Lindqvist U, Westerberg G, Bergstrom M, et al. [^{11}C]Hyaluronan uptake with positron emission tomography in liver disease. Eur J Clin Invest. 2000; 30:600–607. [PubMed: 10886300]
44. Hutchins GD, Schwaigaer M, Rosenspire KC, et al. Noninvasive quantification of regional blood flow in the human heart using N-13 ammonia and dynamic positron emission tomographic imaging. J Am Coll Cardiol. 1990; 15:1032–1042. [PubMed: 2312957]
45. Braun AR, Balkin TJ, Wesenten NJ, et al. Regional cerebral blood flow throughout the sleep-wake cycle. An $H_2{}^{15}O$ PET study. Brain. 1997; 120:1173–1197. [PubMed: 9236630]
46. Mettler, FA.; Guiberteau, MJ. Essentials of Nuclear Medicine Imaging. Saunders Elsevier; Philadelphia, PA: 2006.

47. Bar-Shalom R, Yefremov N, Guralnik L, et al. Clinical performance of PET/CT in evaluation of cancer: additional value for diagnostic imaging and patient management. J Nucl Med. 2003; 44:1200–1209. [PubMed: 12902408]
48. Lardinois D, Weder W, Hany TF, et al. Staging of non–small-cell lung cancer with integrated positron-emission tomography and computed tomography. N Engl J Med. 2003; 348:2500–2507. [PubMed: 12815135]
49. Clément O, Luciani A. Imaging the lymphatic system: possibilities and clinical application. Eur Radiol. 2004; 14:1498–1507. [PubMed: 15007613]
50. Misselwitz B. MR contrast agents in lymph node imaging. Eur J Radiol. 2006; 58:375–382. [PubMed: 16464554]
51. Pan D, Suzuki Y, Yang PC, et al. Indirect magnetic resonance lymphangiography to assess lymphatic function in experimental murine lymphedema. Lymph Res Biol. 2006; 4:211–215.
52. Ruehm SG, Schroeder T, Debatin JF. Interstitial MR lymphography with gadoterate meglumine: initial experience in humans. Radiology. 2001; 220:816–821. [PubMed: 11526287]
53. Lohrmann C, Foeldi E, Langer M. Indirect magnetic resonance lymphangiography in patients with lymphedema: preliminary results in humans. Eur J Radiol. 2006; 59:401–406. [PubMed: 16621396]
54. Lohrmann C, Foeldi E, Bartholomae J-P, et al. Gadoteridol for MR imaging of lymphatic vessels in lymphoedematous patients: initial experience after intracutaneous injection. Br J Radiol. 2007; 80:569–573. [PubMed: 17704317]
55. Lohrmann C, Foeldi E, Speck O, et al. High-resolution MR lymphangiography in patients with primary and secondary lymphedema. Am J Roentgenol. 2006; 187:556–561. [PubMed: 16861563]
56. Matsushima S, Ichiba N, Hayashi D, et al. Nonenhanced magnetic resonance lymphoductography: visualization of lymphatic system of the trunk on 3-dimensional heavily T2-weighted image with 2-dimensional prospective acquisition and correction. J Comput Assist Tomography. 2007; 31:299–302.
57. Bellin MF, Roy C, Kinkel K, et al. Lymph node metastases: safety and effectiveness of MR imaging with ultrasmall superparamagnetic iron oxide particles–initial clinical experience. Radiology. 1998; 207:799–808. [PubMed: 9609907]
58. Réty F, Clement O, Siauve N, et al. MR lymphography using iron oxide nanoparticles in rats: pharmacokinetics in the lymphatic system after intravenous injection. J Magn Res Imaging. 2000; 12:734–739.
59. Sutton, D. Radiology and Imaging for Medical Students. Churchill Livingstone; Edinburgh, UK: 1998.
60. Suresh S, Kumaraswami V, Suresh I, et al. Ultrasonographic diagnosis of subclinical filariasis. J Ultrasound Med. 1997; 16:45–49. [PubMed: 8979226]
61. Mellor RH, Brice G, Stanton AWB, et al. Mutations in FOXC2 are strongly associated with primary valve failure in veins of the lower limb. Circulation. 2007; 115:1912–1920. [PubMed: 17372167]
62. Motomura K, Inaji H, Komoike Y, et al. Gamma probe and ultrasonographically-guided fine-needle aspiration biopsy of sentinel lymph nodes in breast cancer patients. Eur J Surg Oncol. 2001; 27:141–145. [PubMed: 11289748]
63. Bedrosian I, Bedi D, Kuerer HM, et al. Impact of clinicopathological factors on sensitivity of axillary ultrasonography in the detection of axillary nodal metastases in patients with breast cancer. Ann Surg Oncol. 2003; 10:1025–1030. [PubMed: 14597440]
64. Wisner ER, Ferrara KW, Short RE, et al. Sentinel node detection using contrast-enhanced power Doppler ultrasound lymphography. Invest Radiol. 2003; 38:358–365. [PubMed: 12908703]
65. Goldberg BB, Merton DA, Liu J-B, et al. Sentinel lymph nodes in a swine model with melanoma: contrast-enhanced lymphatic US. Radiology. 2004; 230:727–734. [PubMed: 14990839]
66. Hauff P, Reinhardt M, Briel A, et al. Molecular targeting of lymph nodes with L-selectin ligand-specific US contrast agent: a feasibility study in mice and dogs. Radiology. 2004; 231:667–673. [PubMed: 15118116]
67. Lim, H.; Soter, N. Clinical Photomedicine. Marcel Dekker Inc; New York: 1993.

68. Fischer M, Costanzo U, Hoffman U, et al. Flow velocity of cutaneous lymphatic capillaries in patients with primary pymphedema. Microcirculation. 1997; 17:143–149.
69. Mellor RH, Stanton AWB, Azardo P, et al. Enhanced cutaneous lymphatic network in the forearms of women with postmastectomy oedema. J Vasc Res. 2000; 37:501–512. [PubMed: 11146404]
70. McGreevy JM, Cannon MJ, Grissom CB. Minimally invasive lymphatic mapping using fluorescently labeled vitamin B12. J Surg Res. 2003; 111:38–44. [PubMed: 12842446]
71. Parungo CP, Ohnishi S, Kim S, et al. Intraoperative identification of esophageal sentinel lymph nodes with near-infrared fluorescence imaging. J Thorac Cardiovasc Surg. 2005; 129:844–850. [PubMed: 15821653]
72. Kim S, Lim YT, Soletz EG, et al. Near-infrared fluorescent type II quantum dots for sentinel lymph node mapping. Nat Biotechnol. 2004; 22:93–97. [PubMed: 14661026]
73. Parungo CP, Ohnishi S, Kim S, et al. Sentinel lymph node mapping of the pleural space. Chest. 2005; 127:1799–1804. [PubMed: 15888861]
74. Soltesz EG, Kim S, Laurence RG, et al. Intra-operative sentinel lymph node mapping of the lung using near-infrared fluorescent quantum dots. Ann Thorac Surg. 2005; 79:269–277. [PubMed: 15620956]
75. Gurfinkel M, Thompson AB, Ralston W, et al. Pharmacokinetics of ICG and HPPH-car for the detection of normal and tumor tissue using fluorescence, near-infrared reflectance imaging: a case study. Photochem Photobiol. 2000; 72:94–102. [PubMed: 10911733]
76. Sharma R, Wang W, Rasmussen JC, et al. Quantitative imaging of lymph function. Am J Physiol Heart Circ Physiol. 2007; 292:H3109–H3118. [PubMed: 17307997]
77. Swartz MA. The physiology of the lymphatic system. Adv Drug Deliv Rev. 2001; 50:3–20. [PubMed: 11489331]
78. Kitai T, Inomto T, Miwa M, et al. Fluorescence navigation with indocyanine Green for detecting sentinel lymph nodes in breast cancer. Breast Cancer. 2005; 12:211–215. [PubMed: 16110291]
79. Motomura K, Inaji K, Komoike Y, et al. Sentinel node biopsy guided by indocyanin green dye in breast cancer patients. Jpn J Clin Oncol. 1999; 29:604–607. [PubMed: 10721942]
80. Unno N, Inuzuka K, Suzuki M, et al. Preliminary experience with novel fluorescence lymphography using indocyanine green in patients with secondary lymphedema. J Vasc Surg. 2007; 45:1016–1021. [PubMed: 17391894]
81. Sevick-Muraca EM, Sharma R, Rasmussen JC, et al. Imaging of lymph flow in breast cancer patients after microdose administration of a near-infrared fluorophore: feasibility stud. Radiology. 2008; 246:734–741. [PubMed: 18223125]
82. Sampath L, Kwon S, Ke S, et al. Dual-labeled trastuzumab-based imaging agent for the detection of human epidermal growth factor receptor 2 overexpression in breast cancer. J Nucl Med. 2007; 48:1501–1510. [PubMed: 17785729]
83. Houston JP, Ke S, Wang W, et al. Quality analysis of *in vivo* NIR fluorescence and conventional gamma images acquired using a dual-labeled tumor targeting probe. J Biomed Optics. 2005; 10:054010.
84. Kwon S, Sevick-Muraca EM. Noninvasive quantitative imaging of lymph function in mice. Lymphat Res Biol. 2007; 5:219–231. [PubMed: 18370912]
85. Engeset A, Tjotta E. Lymphatic pathways from the tail in rats and mice. Cancer Res. 1960; 20:613–614.
86. Kobayashi H, Kawamoto S, Brechbiel MW, et al. Detection of lymph node involvement in hematologic malignancies using micromagnetic resonance lymphangiography with a gadolinum-labeled dendrimer nanoparticle. Neoplasia. 2005; 7:984–991. [PubMed: 16331884]
87. Kobayashi H, Kawamoto S, Star RA, et al. Micro-magnetic resonance lymphangiography in mice using a novel dendrimer-based magnetic resonance imaging contrast agent. Cancer Res. 2003; 63:271–276. [PubMed: 12543772]
88. Kobayashi H, Kawamoto S, Sakai Y, et al. Lymphatic drainage imaging of breast cancer in mice by micro-magnetic resonance lymphangiography using a nano-sized paramagnetic contrast agent. J Natl Cancer Inst. 2004; 96:703–708. [PubMed: 15126607]
89. Leu AJ, Berk DA, Yuan F, et al. Flow velocity in the superficial lymphatic network of the mouse tail. Am J Physiol Heart Circ Physiol. 1994; 267:H1507–1513.

90. Leu AJ, Berk DA, Lymboussaki A, et al. Absence of functional lymphatics within a murine sarcoma: a molecular and functional evaluation. Cancer Res. 2000; 60:4324–4327. [PubMed: 10969769]
91. Swartz MA, Berk DA, Jain RK. Transport in lymphatic capillaries. 1 Macroscopic measurements using residence time distribution theory. Am J Physiol. 1996; 270:H324–H329. [PubMed: 8769768]
92. Slavin SA, Van den Abbeele AD, Losken A, et al. Return of lymphatic function after flap transfer for acute lymphedema. Ann Surg. 1999; 229:421–427. [PubMed: 10077056]
93. Ballou B, Ernst LA, Andreko S, et al. Sentinel lymph node imaging using quantum dots in mouse tumor models. Bioconjug Chem. 2007; 18:389–396. [PubMed: 17263568]
94. Hama Y, Koyama Y, Bernardo M, et al. Spectral near-infrared fluorescence imaging of curved surfaces using projection reconstruction algorithms. Contrast Media Mol Imaging. 2007; 2:82–87. [PubMed: 17451166]
95. Wunderbaldinger P, Turetschek K, Bremer C. Near-infrared fluorescence imaging of lymph nodes using a new enzyme sensing activatable macro-molecular optical probe. Eur Radiol. 2003; 13:2206–2211. [PubMed: 12802615]
96. Kersey TW, Eyk JV, Lannin DR, et al. Comparison of intradermal and subcutaneous injections in lymphatic mapping. J Surg Res. 2001; 96:255–259. [PubMed: 11266281]
97. Hammer JB, Flemming MD. Lymphedema therapy reduces the volume of edema and pain in patients with breast cancer. Ann Surg Oncol. 2007; 14:1904–1908. [PubMed: 17342565]
98. Schledzewski K, Falkowski M, Moldenhauer G, et al. Lymphatic endothelium-specific hyaluronan receptor LYVE-1 is expressed by stabilin-1(+), F4/80(+), CD11b(+) macrophages in malignant tumours and wound healing tissue *in vivo* and in bone marrow cultures *in vitro*: implications for the assessment of lymphagiogenesis. J Pathol. 2006; 209:67–77. [PubMed: 16482496]
99. Karkkainen MJ, Mäkinen T, Alitalo K. Lymphatic endothelium: a new frontier of metastasis research. Nat Cell Biol. 2002; 4:E2–E5. [PubMed: 11780131]
100. Banerji S, Ni J, Wang S-X, et al. LYVE-1, a new homologue of CD44 glycoprotein, is a lymph specific receptor for hyaluronan. J Cell Biol. 1999; 144:789–801. [PubMed: 10037799]
101. Koukourakis MI, Giatromanolaki A, Sivridis E, et al. LYVE-1 immunohistochemical assessment of lymphangiogenesis in endometrial and lung cancer. J Clin Pathol. 2005; 58:202–206. [PubMed: 15677543]
102. Nathanson SD. Insights into the mechanisms of lymph node metastasis. Cancer. 2003; 98:413–423. [PubMed: 12872364]
103. Jackson DG. Biology of the lymphatic marker LYVE-1 and applications in research into lymphatic trafficking and lymphangiogenesis. APMIS: Acta Pathol Microbiol Immunol. 2004; 112:526–538.
104. Liu NF. Trafficking of hyaluronan in the interstitium and its possible implications. Lymphology. 2004; 37:6–14. [PubMed: 15109072]
105. Laurent TC, Fraser JRE. Hyaluronan. FASEB J. 1992; 6:2397–2404. [PubMed: 1563592]
106. Liu NF, Zhang LR. Changes of tissue fluid hyaluronan (hyaluronic acid) in peripheral lymphedema. Lymphology. 1998; 31:173–179. [PubMed: 9949388]
107. Armstrong SE, Bell DR. Relationship between lymph and tissue hyaluronan in skin and skeletal muscle. Am J Physiol Heart Circ Physiol. 2002; 283:H2485–H2494. [PubMed: 12388305]
108. Kitayama J, Ishigami H, Ishikawa M, et al. Hyaluronic acid is a useful tool for intraoperative sentinel node detection in gastric cancer surgery. Surgery. 2007; 141:815–820. [PubMed: 17560258]

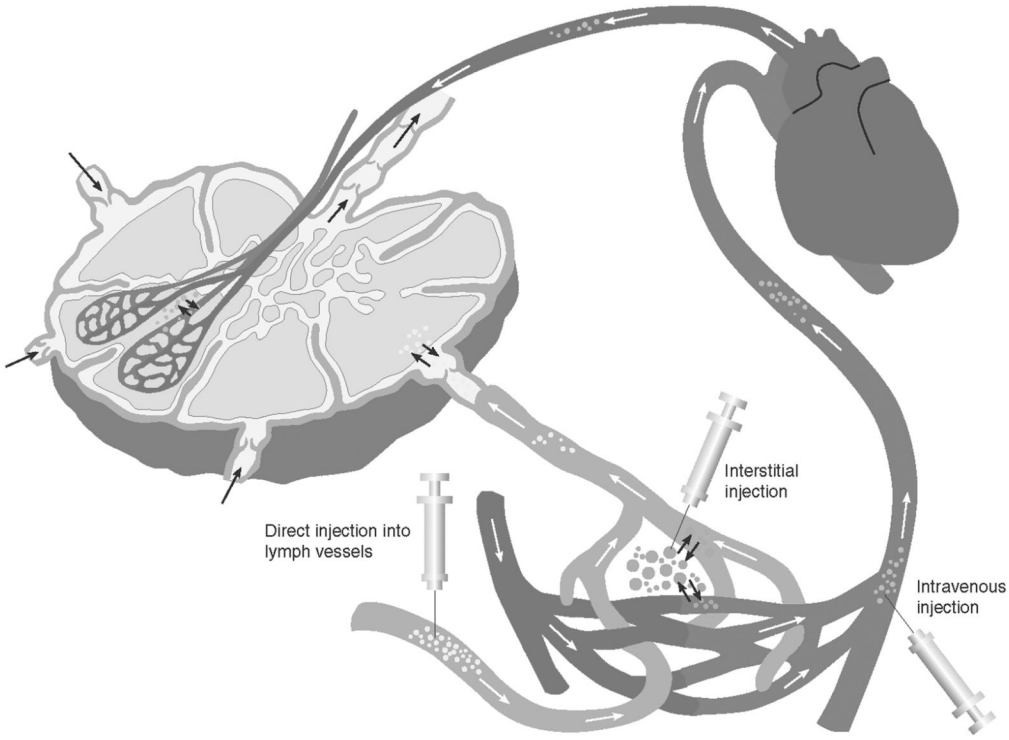

FIGURE 1.
Injection routes to introduce contrast agents into the lymphatics are through interstitial (intradermal or subcutaneous) administration, direct administration into a cannulated lymphatic vessel, or intravenous injection.

FIGURE 2.

An X-ray radiograph depicts lymphatics and lymphatic fistula in a patient who underwent resection of melanoma of right thigh and inguinal lymphadenectomy. The *arrow* indicates Lipidiol leakage. Pedal lymphangiography was performed after injection of 14 mL of Lipidiol iodinated glycerol ester. (From Kos *et al.*[12] Reproduced by permission.)

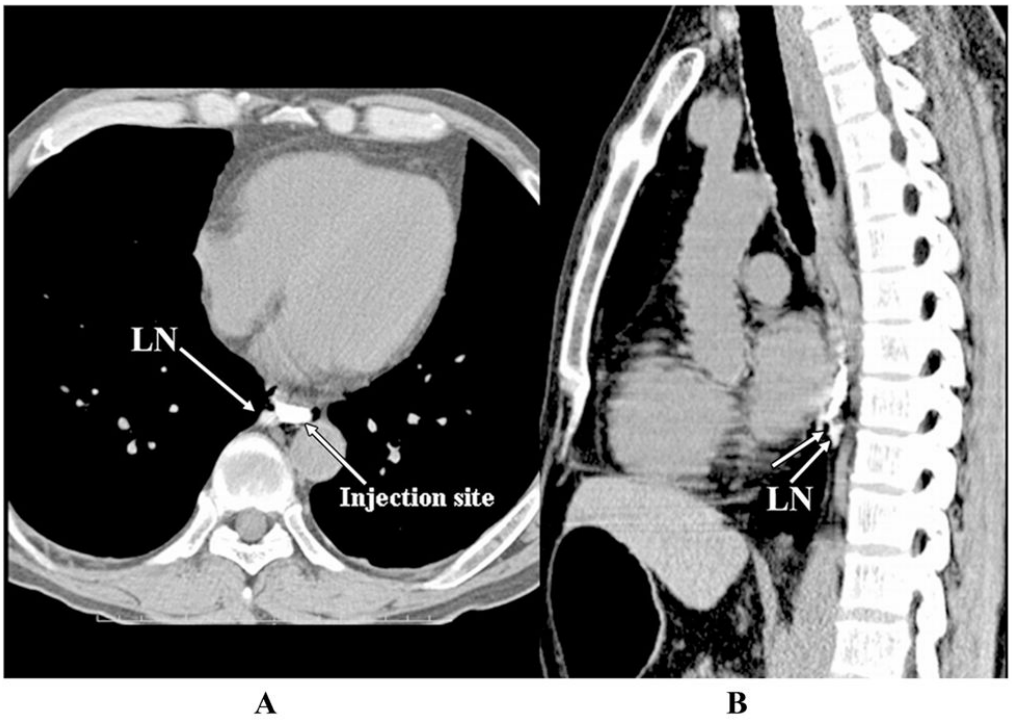

FIGURE 3.
Transverse (**A**) and sagittal (**B**) endoscopic contrast-enhanced CT lymphangiograms of a patient with esophageal cancer injected peritumorally with 2 mL of iopamidol. The images identify short lymphatic vessel (*unlabeled arrow* in B) and a paraesophageal lymph node. (From Suga *et al.*[22] Reproduced by permission.)

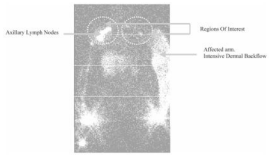

FIGURE 4.
Lymphoscintigram of a postmastectomy lymphedema patient. The affected arm depicts dermal backflow as compared to the unaffected arm that shows a channel draining the injection site to the axillary lymph nodes. (From Szuba *et al.*[32] Reproduced by permission.)

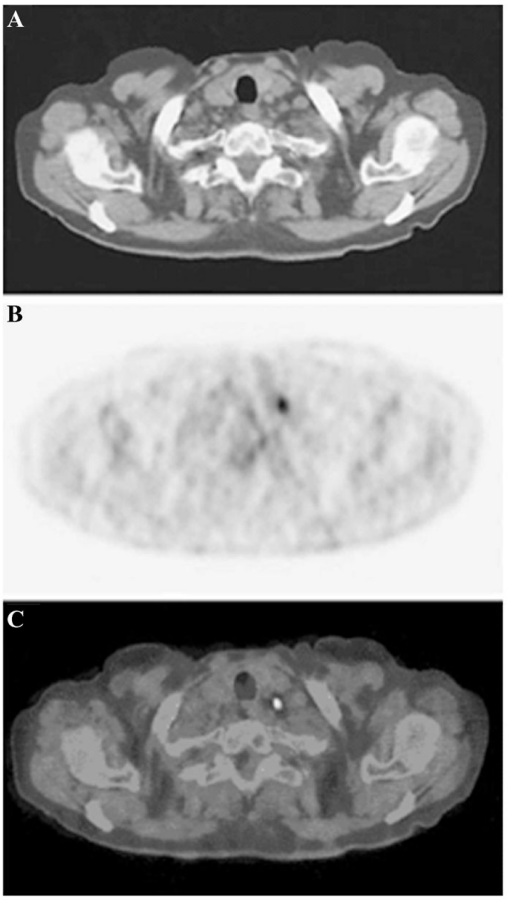

FIGURE 5.
(**A**) Sagittal CT scan, (**B**) PET scan, and (**C**) coregistered PET-CT scan of a patient with non–small cell lung cancer after intravenous injection of 350–400 MBq of 18-FDG. (From Lardinois *et al.*[48] Reproduced by permission.)

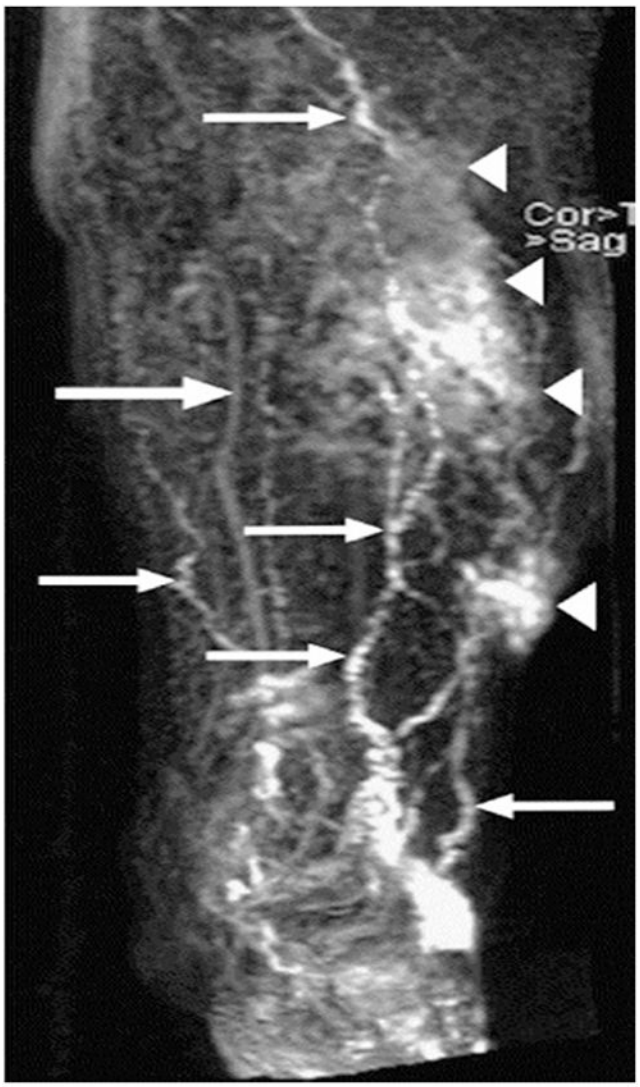

FIGURE 6.
Enlarged lymphatic vessels (*small arrows*), dermal backflow (*arrowheads*), and concomitantly enhanced veins (*large arrow*) in the lower left part of the leg of a 69-year-old man with primary lymphedema. The image was acquired 35 min after gadodiamide injection. (From Lohrmann *et al*.[53] Reproduced by permission.)

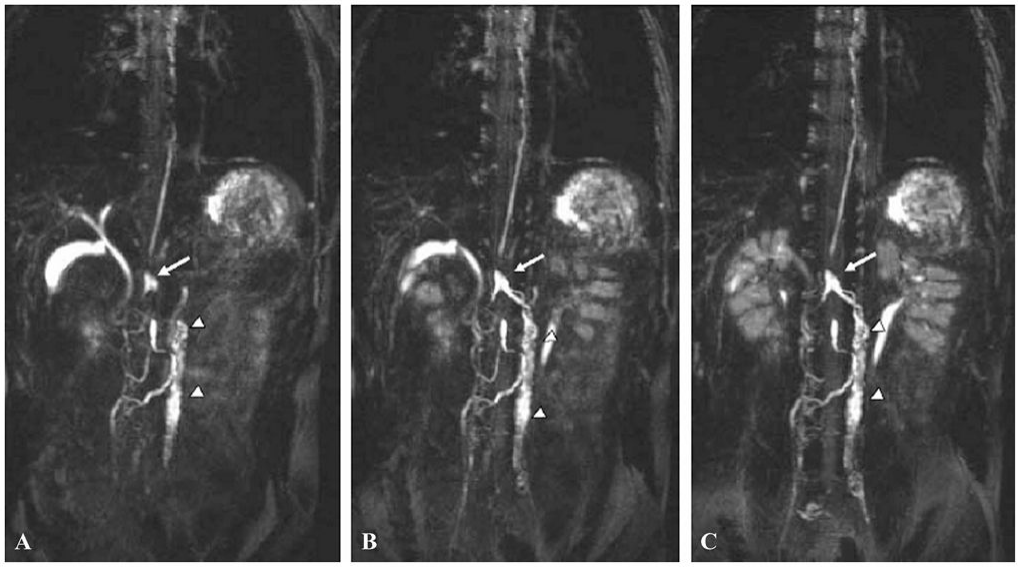

FIGURE 7.

Coronal maximum intensity projection images of a 28-year-old male. Three dimensional heavily T2-weighted images were obtained in the expiratory phase when the diaphragm was at the highest level. (**A** to **C**) A high intensity linear structure clearly identifies thoracic duct. *Arrows* identify a saccular structure to be cysterna chili, and *arrowheads* indicate lumbar lymphatics and para-aortic lymphatic trunks. The lymphatics were solely identified on the basis of the knowledge of systemic anatomy. (From Matsushima *et al.*[56] Reproduced by permission.)

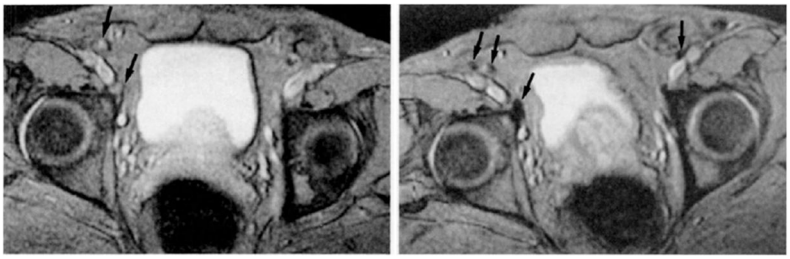

FIGURE 8.
MR images depict benign iliac lymph nodes in a patient with prostatic carcinoma. (**A**) Precontrast image of external iliac lymph nodes. *Arrows* indicate iliac lymph nodes that appear bright on account of high signal intensity. (**B**) Postcontrast image of iliac lymph nodes (*arrows*) that appear to be dark because of the accumulation of USPIO. Contrast-enhanced MR images are acquired after injection of 1.7 Fe/kg USPIO. (From Bellin *et al.*[57] Reproduced by permission.)

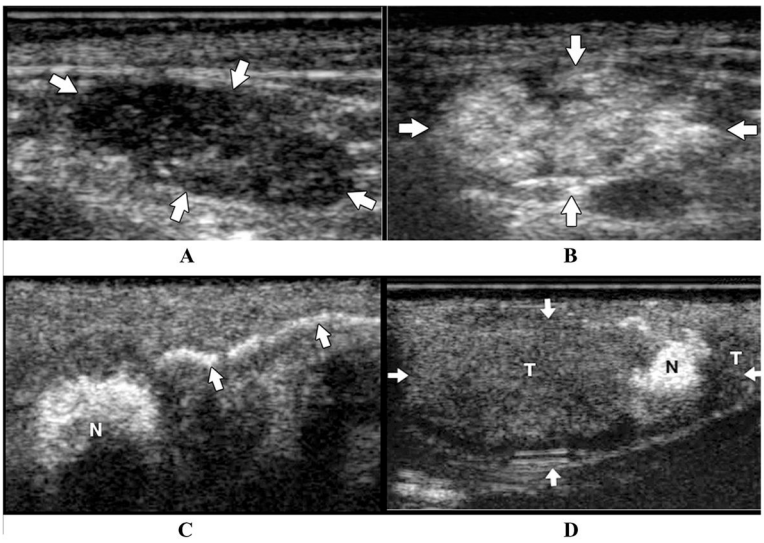

FIGURE 9.

US scans of a normal and malignant lymph nodes pre- and postcontrast subcutaneous administration in a swine model of melanoma. (**A**) Precontrast US image depict hypoechoic ellipsoid lymph node; (**B**) postcontrast US scans depict hyperechoic lymph nodes; (**C**) contrast-enhanced lymph channel draining into a sentinel lymph node (N) subsequent to an intradermal injection of microbubbles; (**D**) postcontrast US scan of a lymph node (*arrows*) composed of hypoechoic region depicting buildup of melanoma tumor cells (T), with a small region of normal tissue (N) that demonstrates contrast enhancement. (From Goldberg *et al.*[65] Reproduced by permission.)

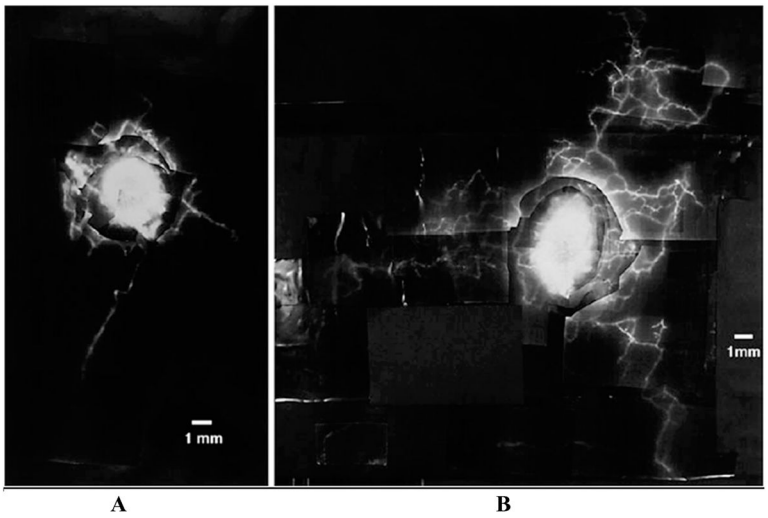

FIGURE 10.
Fluorescence lymphangiogram of a lymphedematous arm depicts denser lymphatic network as opposed to that in normal lymphatics in a postmastectomy lymphedema patient. (**A**) Lymphatics in affected limb; (**B**) lymphatics of affected arm of a postmastectomy patient with edema. Ten microliters of 25% (w/v) fluorescein isothiocyanate was injected into the dermis on the ventral aspect of the forearm. (From Mellor *et al.*[69] Reproduced by permission of S. Karger AG.)

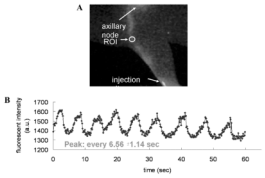

FIGURE 11.

NIR optical imaging enables detection of pulsatile lymph flow in mice. (**A**) Fluorescence image; (**B**) intensity profile as a function of time in a specific ROI along a lymph vessel after intradermal injection of 2 μL of 1.29 μM IC-Green in dorsal aspect of paw. The intensity profile shows that the peak fluorescence occurs at an average of every 6.56 ± 1.14 s. (From Kwon and Sevick-Muraca[84] Reproduced by permission.)

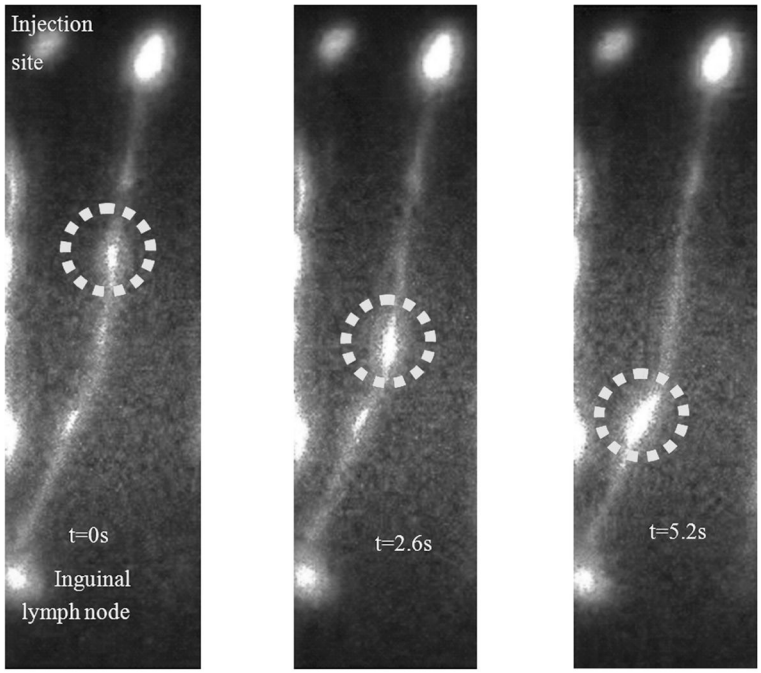

FIGURE 12.
Fluorescent images depict a bolus of IC-Green (*circle*) transiting along a swine's abdominal lymph channel at (left) $t = 0$, (middle) $t = 2.6$, and (right) $t = 5.6$ s. The lymphatic channel drained to the swine's inguinal region.

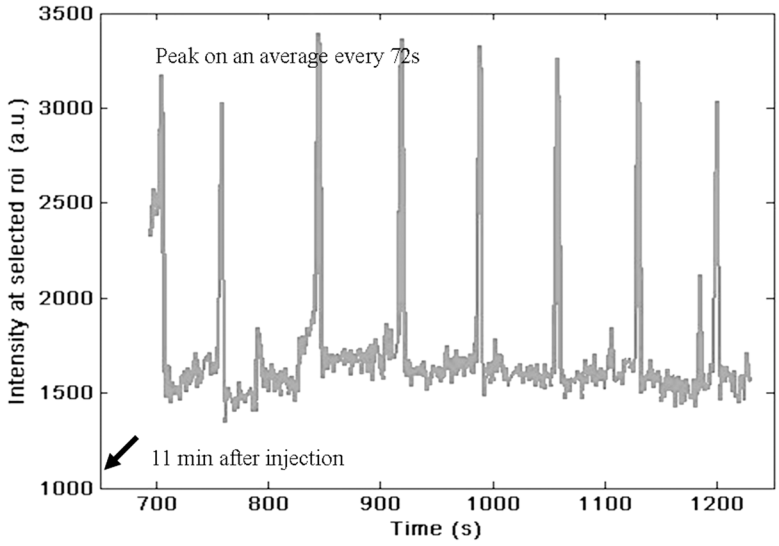

FIGURE 13.

Plot of mean NIR fluorescent intensity profile of a ROI selected on a swine's abdominal lymphatic vessel as a function of imaging time. Consistent peaks that appear on average every 72 s are observed 11 min after intradermal injection of 200 μL of 32 μM IC-Green and indicate pulsatile lymph flow in swine abdomen.

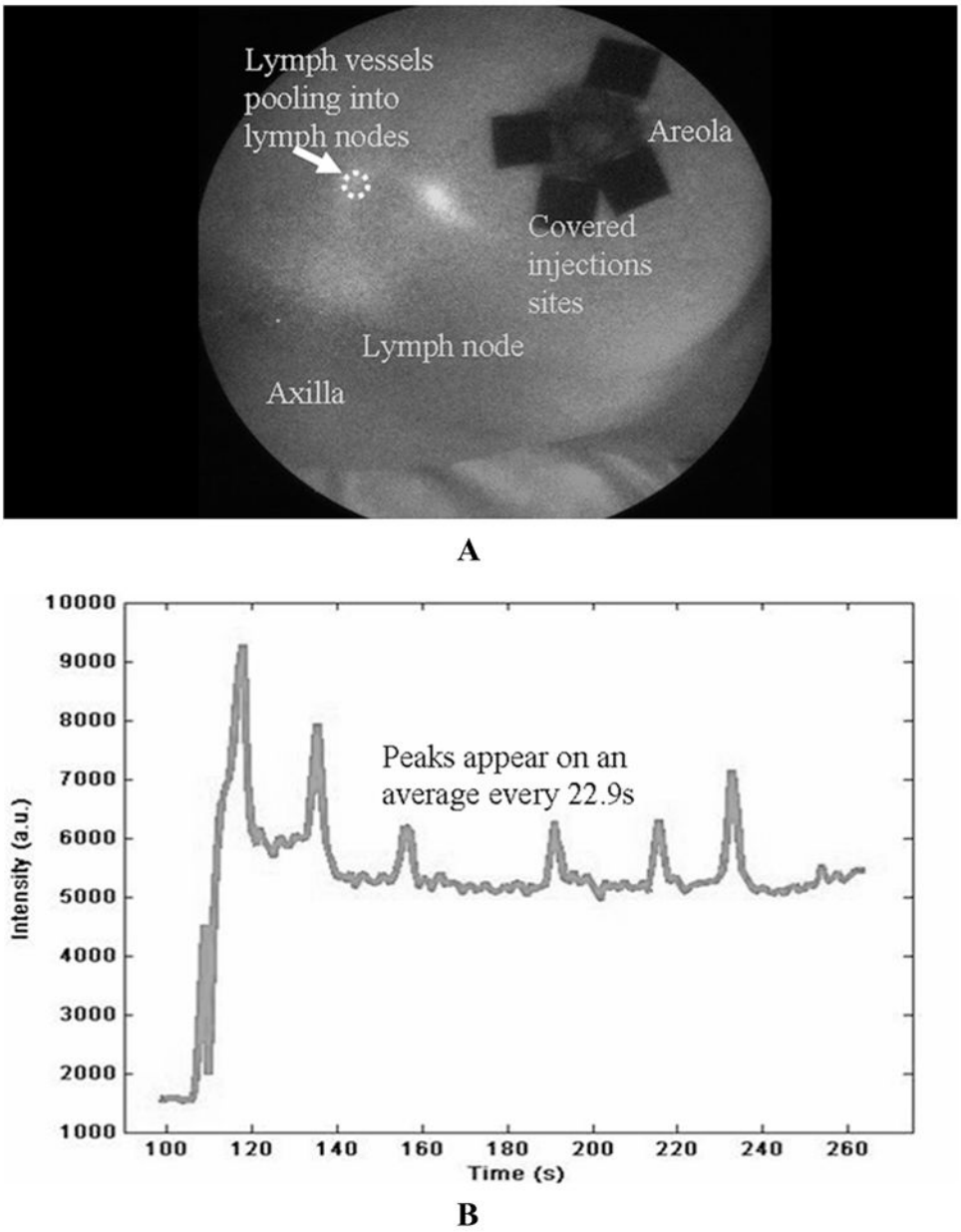

FIGURE 14.

NIR optical lymph imaging detects pulsatile flow in humans. (**A**) White-light and NIR fluorescent image overlay of a subject with breast cancer. Intradermal injection is performed with 100 μL of 20 μg IC-Green in the peri-areolar region on the right breast. *Arrow* identifies a lymph channel on patient's left breast. (**B**) Plot of intensity profile at a ROI (*oval* in **A**) as a function of duration of image acquisition. The peaks indicate that lymph channel conducts the bolus of IC-Green from the injection site to axilla on an average every 22.9 ± 7.8 s.

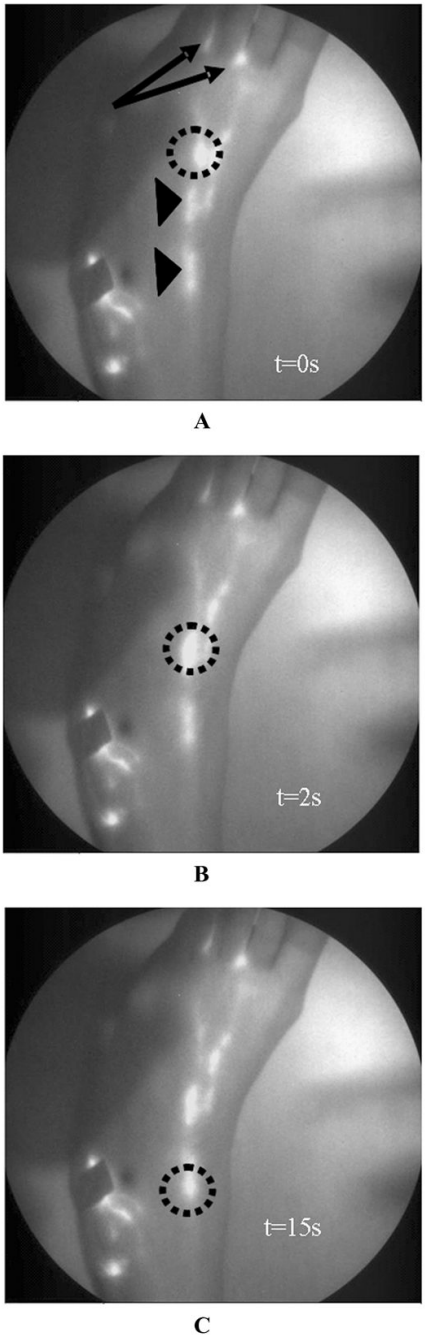

FIGURE 15.

White-light overlay with corresponding fluorescent images of lymphatic map of foot of a 46-year-old female who was injected with 100 μL of 25 μg of IC-Green in the first and second interdigital spaces (*arrows*) in the dorsum of the foot. *Circles* indicate a "packet" of dye transiting along the lymphatic channel. *Arrowheads* identify localized collection of fluorescent dye that could be lymphangions of a lymphatic vessel. Panels **A**, **B** and **C** depict images at 0,2, and 15 s.

FIGURE 16.
A white-light and fluorescent overlay image of lymphatics in a human hand. A 22-year-old male was injected with 100 μL of 25 μg of IC-Green in the four interdigital spaces on the right hand. Five discrete lymphatics appear to drain the dye from the injection site up to the axilla.

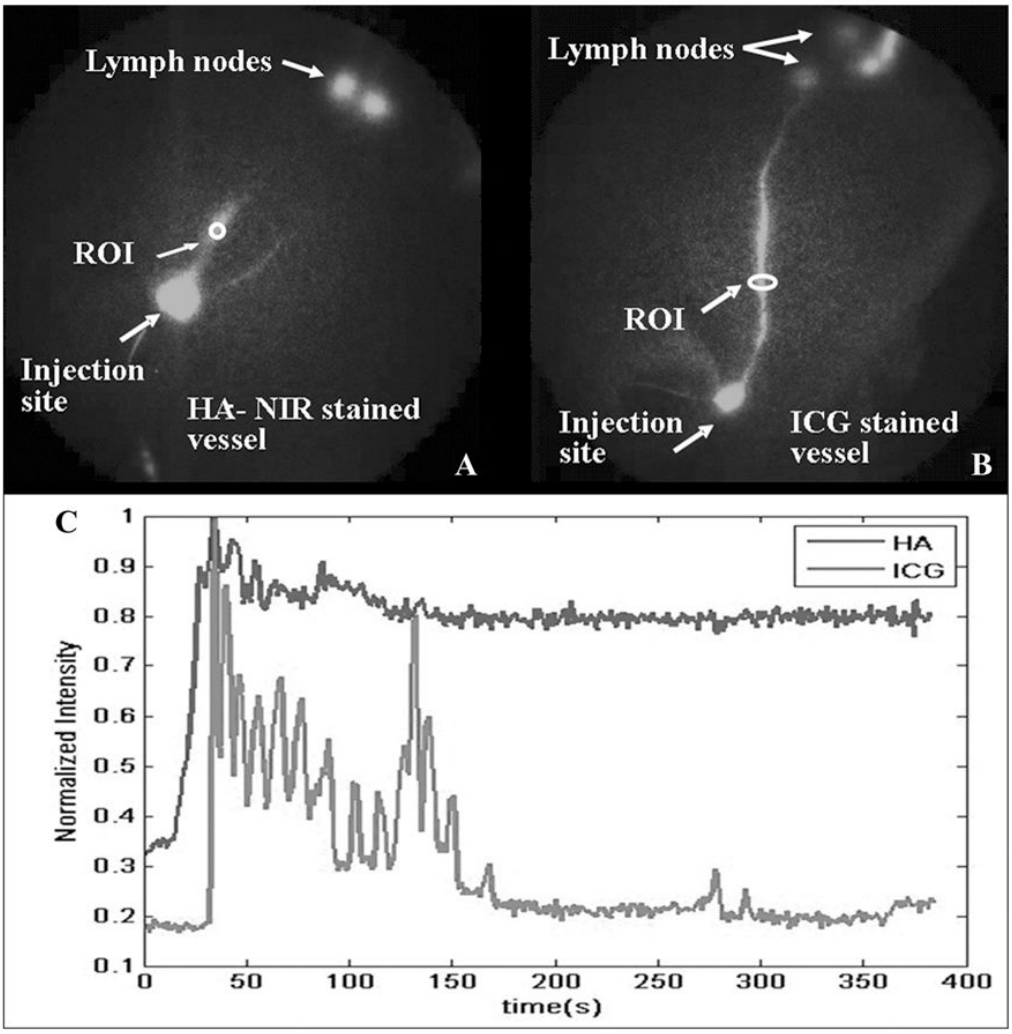

FIGURE 17.

A plot of mean fluorescent intensity of leg lymph vessel stained with HA-NIR and IC-Green at ROIs (*ovals*) for duration of image acquisition. (**A)** Oval indicates an ROI selected on leg lymph vessel stained with HA-NIR dye. (**B**) Oval identifies an ROI on leg lymph vessel with trafficking IC-Green, and (**C**) comparison of intensity profile as a function of time for selected ROIs. (From Sharma *et al.*[76] Reproduced by permission.)